Design and performance prediction of radial ORC turboexpanders

Performance prediction of radial ORC Turboexpanders

Daniele Fiaschi(*), Giampaolo Manfrida, Francesco Maraschiello

Università degli Studi di Firenze, Dipartimento di Ingegneria Industriale

Viale Morgagni 40/44 50134, Firenze Italy

Email: daniele.fiaschi@unifi.it

francesco.maraschiello@unifi.it

giampaolo.manfrida@unifi.it

Abstract

In this paper, a zero-dimensional model for the design of radial Turbo-Expanders for ORC applications is discussed, with special reference to the estimation of losses and efficiency; a comparison between different fluids (R134a, R1234yf, R236fa, R245fa, Cyclo-Hexane, N-Pentane) is presented and discussed, referring to a typical small-size application (50 kW). In the model, different methods for the design of radial turbines are screened, with special attention to the estimation of losses, for which correlations from literature are used. Real Equations Of State (EOS) are applied to the expansion process in place of the traditionally adopted Mach relationships for ideal gas, which is a significant advancement for modeling organic fluids in ORC, often operating near to critical conditions. The results show that the total to total efficiency of the designed machines range between 0.72 and 0.80, depending on the considered fluid. Generally, higher efficiency (1.5 – 2.5 % points) can be achieved adopting backswept-bladed rotors. The most significant losses come from the rotor secondary flows , due to the high curvature of blade profiles combined to the large pressure gradient. The best performing fluids are R236fa and R245fa, followed by R134a and R1234yf.

Finally, starting from the developed design tool, an off-design analysis of turbo-expanders is presented. Once the design data are available, the characteristic curves of the expander at variable temperature, pressure and fluid mass flowrate at the expander inlet for different values of the specific speed are built. It is thus possible to evaluate the performance of the radial expanders when working far from design point. This analysis, demonstrated for R134a, shows that the total to static

(*)Corresponding Author

efficiency has a relatively modest sensitivity to the off design of the expansion ratio, especially at corrected speed below the design value.

Keywords
Radial Turbine Design, Expansion Efficiency Losses, Off design, Micro ORC

1. Introduction

Organic Rankine Power Cycles (ORC) are becoming a leading technology for energy conversion, with special reference to low size (< 100 kW) and low-temperature applications (T<150°C), where the use of steam is not convenient. The thermodynamic properties of organic fluids make them very interesting for small/medium size power plants (50 to 5000 kW or more, at present); applications of ORC cycles range from heat recovery at gas turbine discharge [1, 2, 3] or internal combustion engines [4, 5], to energy conversion from biomass [6], solar [7, 8, 9], and geothermal resources [10, 11, 12]. Due to the low working temperature, ORCs have typically low efficiency levels: for this reason, the accurate design of the expander is a very important issue to avoid further appreciable reduction of performance. For these applications and power range, radial (or mixed flow) turbines are usually preferred to the axial ones, because they offer several advantages: a low degree of reaction (thereby simplifying sealing), capability of dealing with large enthalpy drops with relatively low peripheral speeds, possibility of adopting a single-stage design. On the whole, this results in good performance and affordable price. The optimization of the thermodynamic cycle, with special reference to fluid selection, has been studied widely in the last years. Fluid-dynamic design of turbo-expanders can take advantage of the availability of modern CFD methods [….]; however, there is a need for preliminary design methods, and of modeling tools capable of predicting the off-design performance (which is determined, for example, by the variation of the resource for solar-driven EGS, or by variation of ambient temperature in geothermal or heat recovery applications). In the field of low power output (i.e. up to 100 – 150 kW), radial expanders are almost the only choice, with the eventual competition of screw expanders. Generally, literature is rich of theoretical – experimental correlations for the estimation of losses in axial expanders, whereas much less data are available for radial turbines [13 – 30]. Most data available refer to ideal gas and make use of the Mach compressibility relations [13-20]. This may not be a satisfactory approximation when dealing with ORC turbines, which operate near the saturation line or close to the critical point. In the model hereafter proposed, correlations from literature are used [13-30], but real Equations Of State (EOS) are applied to the expansion process (static and total variables) in

place of ideal gas relations. This is an important feature, allowing to preliminary design and performance prediction of turbo-expanders that work with real substances. The correlations can be refined progressively as more data on ORC expanders become available, either from field operation, or from specific test arrangements. The thermodynamic properties of theworking fluids are calculated using the libraries of the EES software, which is the programming environment adopted in this work. Making use of the design model, a sensitivity analysis investigating the effects of the different design parameters on the expander performance is presented. Finally, an off-design model has been developed and some results are discussed, in order to assess the behavior and estimate the performance of the turbo-expanders when working out of nominal conditions. This often happens when the ORC high-temperature resource is a time-dependent energy source, like solar; but also, with seasonal change of condenser conditions, on account of the heat/mass transfer performance of the cooling system (condenser/cooling tower/air cooler).

2. Fundamental design concepts and parameters for Radial-Inflow Turbines (IFR)

Radial-inflow turbines have been less studied than the axial ones, and have been manufactured by a limited number of companies [31, 32, 33].The fundamental design of radial-inflow turbines is presented and discussed in books and scientific papers [13-30], most of which are based on experimental work performed at NASA between 1965 and 1975 [16, 17, 18, 20, 30]. At that time radial turbines, working with ideal gases (air, helium), were designed and tested for aerospace applications. The high values of centrifugal stresses on rotor blades and the limits on materials performance and production technology led to the design of the ideal 90° IFR turbine: that is, a rotor having radial blades at inlet. Some years later (1983) NASA researchers [18] studied and developed a radial – inflow turbine with a more performing rotor design, characterized by a blade sweep angle b_2 at rotor inlet (IFG, figure 1).The typical velocity triangles are shown in figure 2; in both cases, the absolute velocity c_3 is assumed to result axial at rotor outlet, in order to guarantee good diffuser performance (figure 2). Generally, nominal design conditions are referred to zero-incidence at rotor inlet and zero-deviation at rotor outlet; however, in radial turbines, the best efficiency values are obtained when incidence is non-zero (figure 3): this is a consequence of the rotational flow, which displaces the tangential component of the relative velocity (w_u) in the opposite direction with respect to the peripheral rotor velocity. From the technical literature [13, 14] it appears that the best values of rotor inlet angle in the relative flow are between – 20° and – 40° , referred to the camber line direction (the positive sign is conventionally assumed toward the direction of peripheral velocity u).

In radial turbine design, some non – dimensional parameters help designers to select a geometry optimizing efficiency using a limited set of variables; the following parameters are recommended in the literature [13, 14, 17, 19, 20]:

$$\frac{d_{3h}}{d_{3s}} = 0.40 \qquad (1)$$

$$\frac{d_{3s}}{d_2} = 0.70 \qquad (2)$$

Another important parameter is the *isentropic velocity ratio* (u_2/c_s), which maximizes the efficiency in the range 0.69 – 0.71 [13, 14, 17, 19, 20]. c_s is the *spouting velocity*, defined as the velocity at which the kinetic energy of the flow is equal to the isentropic enthalpy drop from turbine inlet stagnation pressure p_{01} to the final exhaust pressure [14]. The definition of spouting velocity is different depending on (I) whether a diffuser is present or not downstream the turbine, see relationships (3) and (4, 5) respectively, and (II) if total (4) or static (5) conditions are considered at the turbine exit (figure 4):

$$c_s = \sqrt{2(h_{01} - h_{4ss})} \qquad (3)$$

$$c_s = \sqrt{2(h_{01} - h_{03ss})} \qquad (4)$$

$$c_s = \sqrt{2(h_{01} - h_{3ss})} \qquad (5)$$

3. Design Guidelines

3.1 Input data and expected process output

The input data consist in the expander rated power output, in the thermo-fluid dynamic variables determined by the thermodynamic cycle [36], and in a set of dimensional and non – dimensional parameters chosen by the designer (table 1)..The outputs of the calculations are the basic geometry with the related velocity triangles and the efficiency of the designed expander. The model is also able to calculate the turbine losses and their relative share in the resulting inefficiency.

3.2 Preliminary sizing

The first step is the preliminary calculation of geometry, using the non – dimensional parameters listed in table 1, which determine also the isentropic nozzle and rotor enthalpy variations. The load and flow coefficients ($\Psi = \Delta h_0/u_2^2$ and $\Phi = c_{m2}/u_2$ respectively) are adjusted to calculate the

peripheral velocity (u_2), specific speed (n_s), speed of revolution (ω) and meridional component of absolute velocity at nozzle exit/rotor inlet (c_{m2}).These data are used for the evaluation of the mass flow rate $\dot{m}$:

$$\dot{m} = \rho_2 c_{m2} b_2 d_2 \pi (1 - BK_2) \qquad (6)$$

The meridional component of the absolute velocity at nozzle inlet (c_{m1}) - which is the same as absolute velocity (c_1) as the flow at the IGV nozzle inlet is assumed to be radial - is given by the application of mass balance in section 1 (figure 1):

$$c_{m1} = \frac{\dot{m}}{\rho_1 \pi b_1 d_1 (1 - BK_1)} \qquad (7)$$

Consequently, knowing the inlet enthalpy $h_1(p_1, T_1)$, it is possible to calculate the total enthalpy (h_{01}). The thermodynamic variables at point 2 (p_2, T_2, h_2, s_2, ρ_2, Ma_2, $Ma_{u2} = \frac{u_2}{VS_2}$, $Ma_{r2} = \frac{w_2}{VS_2}$) and the velocity triangles at rotor inlet are determined calculating first the nozzle isentropic expansion and then the real transformation using the nozzle loss coefficient ξ_N (figure 2):

$$h_2 = h_{2s} + 0.5 \xi_N c_2^2 \qquad (8)$$

Once the nozzle exit/rotor inlet conditions are known, the thermodynamic variables at point 3 (rotor exit/diffuser inlet, figure 1) are calculated by solving at first the rotor isentropic expansion and assuming that the difference between the absolute velocities related to isentropic and real expansion at that point is negligible. The relative velocity at rotor output can be calculated by the conservation of rothalpy [14], figure 2:

$$i = h + 0.5 w^2 - 0.5 u^2 \qquad (9)$$

The meridional component of the absolute velocity at point 3 is determined by the conservation of mass (figure 2):

$$\dot{m} = \rho_3 c_{m3} \frac{{d_{3s}}^2 - {d_{3h}}^2}{4} \pi (1 - BK_3) \qquad (10)$$

Finally, using the rotor loss coefficient and assuming an axial discharge at rotor outlet, the static enthalpy and velocity triangles at rotor outlet can be calculated:

$$h_3 = h_{3s} + 0.5 \xi_R w_3^2 \qquad (11)$$

The calculation of the real conditions at diffuser outlet is done by combining the total enthalpy balance and the definition of diffuser loss coefficient ξ_D.

3.3 Geometry of the stator (IGV)

The prediction of the angle of flow leaving the bladed nozzle of a radial turbine, discussed in the previous section, is a fundamental design topic. The next step is the calculation of the angles of blades, which are radial at inlet for no pre swirled IGVs. At outlet, while leaving the nozzle, the flow does not follow the vanes completely but it turns toward the meridional direction of an angle known as deviation, due to the combined effects of boundary layer growth (limited by the accelerating flow) and the subsequent abrupt expansion due to the trailing edge thickness. As a simple design approach, the actual angle of blades at nozzle outlet is calculated interpolating data from Hiett and Johnston [13, 29], which have a rather linear behavior, approximated by the interpolating function $\alpha_{b2} = 0.884 \cdot \alpha_{b2} + 4.56$.

Another important parameter is the number of stator blades, which directly influences the losses. Increasing the number of blades leads to better flow guidance at the price of higher frictional losses. A general design approach to define the stator number of blades is that it should be a prime number compared to the rotor one. In addition to this basic criterion, the criterion of Zweifel on the optimal ratio between the chord and the blade spacing can be adopted [14; 23]. It suggests that, in order to minimize the losses, the ratio between the tangential load of an actual to that of an ideal blade (Ψ_T) should be about 0.80 Knowing the absolute flow angles at nozzle inlet and outlet, and after calculating the chord length, from the expression of blade pitch $Z \cdot s = \pi \cdot d_2$, the following equation (12) gives the optimum blade spacing, from which the number of blades can be easily determined:

$$\Psi_T = 2\left(\frac{s}{x}\right) cos^2\alpha_2(tan\alpha_1 + tan\alpha_2) \qquad (12).$$

3.4 Optimal incidence at rotor inlet and number of rotor blades

Calculating the number of rotor blades is a fundamental issue in the design of radial turbines, because it defines the basic structure of the machine and has a primary role in the estimation of losses. There are no absolute criteria allowing an univocal evaluation of number of blades; the design guidelines tend to avoid very low local velocities near the blade surface in the inlet region of the rotor, with a consequent tendency to early separation [13]. On the other hand, the adoption of a high number of blades is not so convenient, especially for small rotors: the blockage effects, the weight and inertia of the rotor become very high. Moreover, a large number of blades is also

184 responsible for a large wetted surface area, which increasesthe friction losses. In the present model,
185 rather than using the formulation proposed by Jamieson [14, 15], which determines an exceedingly
186 large number of rotor blades, the formulation proposed by

187 Glassman [16] is followed:

188 $$Z_R = \frac{\pi}{30}(110 - \alpha_2)\, tan\alpha_2 \qquad (14).$$

189 Once the number of blades is determined, the optimum rotor incidence angle can be calculated. As
190 previously discussed, better efficiency values are achieved when incidence is non-zero. Referring to
191 the camber line direction, the best values of rotor inlet angle in relative flow are between 20° and
192 40° counterclockwise.

193 Referring to IFR rotors (radial blades at rotor inlet), the following are the recommended
194 correlations:

195 $$\tan(\beta_{2opt}) = \left(\frac{2}{Z_R}\right)\frac{u_2}{c_{m2}} \qquad (15), [14]$$

196 $$\tan(\beta_{2opt}) = 1 - \frac{0.73\pi}{Z_R} \qquad (16), [13]$$

197 $$\tan(\beta_{2opt}) = \frac{-1.98\tan(\alpha_2)}{Z_R\left(1-\frac{1.98}{Z_R}\right)} \qquad (17), [13]$$

198 The above equations (15 – 17) provide similar results, even though (16) has been obtained
199 considering minimum Mach number conditions at the rotor inlet [13]. From these relationships, one
200 can notice that the optimum rotor incidence angle depends on the number of rotor blades and on the
201 kinematic conditions of flow.

202 In the case of the IFG design (non- radial blades at rotor inlet), the procedure suggested by Meitner
203 & Glassman [18] can be followed by calculating first the optimal value of the peripheral component
204 of the absolute velocity:

205 (18), [18].

206 $$c_{u2\,opt} = \begin{cases} u_2\left(\dfrac{\left[1-\sqrt{\cos(\alpha_{b3})}/(\mathrm{Z_R})^{0,7}\right]\left\{1-\left[(r_3/r_2-\varepsilon_{lim})/(1-\varepsilon_{lim})\right]^3\right\}}{1-\frac{tg(\alpha_{b3})}{tg(\alpha_2)}}\right) & if\ \dfrac{r_3}{r_2} > \varepsilon_{lim} \quad (18a), [18] \\ u_2\left(\dfrac{\left[1-\sqrt{\cos(\alpha_{b3})}/(\mathrm{Z_R})^{0,7}\right]}{1-\frac{tg(\alpha_{b3})}{tg(\alpha_2)}}\right) & if\ \dfrac{r_3}{r_2} \le \varepsilon_{lim} \quad (18b), [18] \end{cases}$$

The parameter ε_{lim} can be determined by:

$$\varepsilon_{lim} = \frac{1}{e^{8.16\cos\alpha_{b3}/Z_b}} \quad (19), [18]$$

Once $c_{u2\ opt}$ has been calculated, it is possible to calculate the relative velocity and blade angle as follows:

$$w_{u2\ opt} = c_{u2,opt} - u_2 \quad (20), [18]$$

$$\beta_{2\ opt} = tan^{-1}\left(\frac{w_{u2,opt}}{c_{m2}}\right) \quad (21), [18].$$

3.5 Expander Efficiency, Power Output, Degree of Reaction and Specific Speed

The calculation of the expander efficiency, power output, design degree of reaction and specific speed are following the guidelines in [37], which are briefly recalled for completeness.

The efficiency can be either referred to turbine discharge or including also the diffuser; in the first case, the Total-to-Total and Total-to-Static efficiency are given by:

$$\eta_{tt} = \frac{h_{01}-h_{03}}{h_{01}-h_{03ss}} \quad (22)$$

$$\eta_{ts} = \frac{h_{01}-h_{03}}{h_{01}-h_{3ss}} \quad (23)$$

If the diffuser is included, the Total-to-Static efficiency becomes:

$$\eta_{ts} = \frac{h_{01}-h_{03}}{h_{01}-h_{4ss}} \quad (24)$$

The power output can be calculated by one of the equivalent three following equations:

$$W = \dot{m}(h_{01} - h_{03}) \quad (25)$$

$$W = \dot{m}(u_2 c_{u2} - u_3 c_{u3}) \quad (26)$$

$$W = \frac{1}{2}\dot{m}[(u_2^2 - u_3^2) + (c_2^2 - c_3^2) - (w_2^2 - w_3^2)] \quad (27)$$

The degree of reaction and the specific speed are given by:

$$R = \frac{h_2 - h_3}{h_1 - h_3} \quad (28)$$

$$n_s = \frac{N Q_3^{1/2}}{\Delta h_{0s}^{3/4}} \quad (29)\ [14]$$

where

$$\Delta h_{0s} = h_{01} - h_{03ss} \quad (30)$$

4. Calculation of losses

In order to evaluate the actual performance of a turbomachine, the contributions of different losses must be calculated. This calculation cannot be substituted by advanced CFD methods, because it provides vital information to the designer, about the process of loss buildup determining the final turbomachine performance. On the other hand, advanced CFD is very useful for cross-checking the overall results of the efficiency/loss model, and often to supplement data which would require very detailed (often impossible) measurements.

Generally, the first step of the design procedure considers consequently the effects of losses through appropriate dimensionless coefficients. The related efficiency drop $\Delta\eta$ is then subtracted from the isentropic value to calculate the actual efficiency:

$$\eta_{act} = \eta_s - \Delta\eta \quad (31),\ [13]$$

In this model, the overall loss of the turbine is obtained by the sum of several contributions, each one estimated through correlations which depend on kinematic and geometric parameters. The dimensionless loss coefficients are defined in several ways, and it is important to merge them to a common basis, in order to apply them within the same model and do some reliable comparisons with results from literature. Referring to the jth loss:

$$\xi_j = \frac{h_j - h_{j,is}}{\frac{1}{2} V_j^{\,2}} \quad (32),\ [13]$$

$$\Delta q_j = \frac{h_{0j} - h_{0j,is}}{u_j^2} \quad (33),\ [13]$$

This is the approach followed in the present model: starting from non – dimensional loss coefficients obtained from the correlations, it calculates ξ and the related efficiency drop($\Delta\eta$), for each kind of loss. It allows, in all kinds of expanders and operating conditions, to analyze the

distribution of losses and to investigate how do they affect the overall performance. The so built model provides a reliable basis to improve the design of different kinds of rotors with several possible working fluids.

4.1 Stator losses

The stator losses, which are generally lower than the rotor losses, have been often evaluated with less accuracy in the literature [13, 24]. They are generally based on experimental data and make use of equations for stationary ducts. Referring to the experimental tests of Hiett and Johnston, Benson determined the stator loss coefficients ($\xi_N = 0.05 - 0.15$) [24], showing that they are very small compared to the corresponding values in the rotor. For the estimation of stator losses it is possible to apply Rodger's correlation [13]:

$$\xi_N = \frac{0.05}{Re^{0.2}}\left[\frac{3\, tg\alpha_2}{s/x} + \frac{scos\alpha_2}{b_2}\right] \qquad (35), [13]$$

where:

$$Re = \frac{c_2 b_2}{\nu_2} \qquad (36)$$

4.2 Rotor losses

The flow in the rotor of a radial turbine is subject to a rapid acceleration in the flow direction, and to a turn both in the meridian plane and along the camberline. These effects give rise to a complex pattern of secondary flows. The flow in the rotor of a radial turbine does not result into a high growth of the boundary layer and separation, even though, due to the three dimensional behavior, it develops a significant non uniformity of the total pressure inside the flow channel, which can lead to generation of losses. The probability of this occurrence increases when the blade loading is augmented. In the present model, the losses are divided in different contributions:

- Incidence loss;
- Skin friction loss;
- Tip clearance loss;
- Blade loading loss;
- Disk friction loss.

4.2.1 Rotor Incidence loss

In the actual working conditions of the expander, the incidence angle of the relative flow at rotor inlet is rarely at the optimal value (equations 15 – 17). For this reason, the incidence loss appears. The recommended models for the estimation of rotor incidence loss were developed at NASA [13, 14, 24]. The general approach is to assume that the kinetic energy associated with the variation of the tangential component of the relative velocity with respect to the design value, which is the result of the fluid – blade impact, is converted in internal energy of the fluid, which leads to an increase of entropy. The detailed calculation procedure is reported in [14].The incidence losses may also be calculated using alternative approaches [13], obtained with the same conceptual assumptions and therefore formally similar:

$$\delta h_{0,i} = \frac{w_2^2 sin^2(|\beta_2 - \beta_{2,opt}|)}{2} \qquad (37), [13];$$

$$\delta h_i = \frac{\left(w_2 sin\beta_2 - w_2 sin\beta_{2,opt}\right)^2}{2} \qquad (38), [13].$$

The above discussed methods provide similar results, consistent with the literature. Thus, any of the two proposed correlations may be adopted leading to negligible differences.

4.2.2 Friction losses

Friction losses can be estimated referring to a rotor-equivalent duct working on the same flow rate [26]:

$$\xi_{R,f} = \frac{\lambda_R L_R^*}{D_R^*} \qquad (39)$$

Details about the calculation of the characteristic diameter and length can be found in [24] or [26]. As for the stator, the friction factor can be determined using Moody's diagram. The relative roughness and Reynolds number are estimated referring to the rotor-equivalent duct. Alternatively to equation (39), the frictional losses may be calculated using the following expression:

$$\Delta q_{R,f} = \frac{4\lambda_R\left[(w_2/VS_{01})^2 + (w_3/VS_{01})^2\right]}{4\left(D_R^*/L_R^*\right)(u_2/VS_{01})^2} \qquad (40), [13].$$

or

This correlationtends, generally, to overestimate the friction losses by 70 – 80%.

4.2.3 Tip clearance losses

Tip clearance losses are due to the fluid leaking through the clearance gaps between the blade tips and the shroud. With reference to the blade geometry, in radial turbines two different types of clearances can be distinguished from the construction point of view: axial at inlet and radial at outlet [30, 38]. However, there is not a net distinction between the two kinds of clearance, but a gradual and continuous change (figure 5). Referring to studies performed at NASA [30] and more recent CFD calculations [38], it may be affirmed that the contribution of radial clearance to the overall loss is almost one order of magnitude higher than the axial one [13, 15, 30, 38].

Several different correlations have been proposed for tip clearance losses, some of which are specific for radial inflow turbines […] and others are derived from centrifugal compressors […]. A wide spread in the results can be produced using different models. Here, the model of Rodgers [13] is proposed:

$$\Delta q_{R,cl} = 0.4 \left(\frac{\varepsilon}{b_2}\right) \left(\frac{c_{u2}}{u_{t,le}}\right)^2 \qquad (43)$$

Equations (43) provide low values of clearance losses, which result in poor agreement with literature. Specifically, it happens when the values of axial clearance in equation are used. When the values of radial clearance are adopted, higher agreement with literature results are achieved [30] for equation (43).

4.2.4 Blade loading loss (including secondary flow)

Blade loading loss, including secondary flow, are caused by the high curvature of the profile and the pressure gradient in the rotor vanes. They give the largest contribution to the reduction of the expander efficiency. However, they are not extensively reported and discussed in literature, often because they are threated in combination with other losses using experimental coefficients [18, 24, 28]. The model here proposed evaluates the secondary flow losses through correlations, as functions of kinematic and geometric parameters. For the calculation of blade loading losses, the following correlation proposed by Rodgers can be used [19]:

$$\delta q_{R,bl} = 2\frac{\left(\frac{c_{u2}}{u_{t,le}}\right)^2}{Z_R\frac{z}{r_2}} \qquad (48)$$

Where $z/r_2$is the ratio between the expander axial length and rotor inlet radius[19].

For the calculation of profile losses, another correlation proposed by Rodgers [40] and suitably revised by Whitfield [19] may be adopted:

$$\delta q_{R,p} = 0.5\left(\frac{\frac{b_2}{r_2}+\frac{b_3}{r_2}}{1-\left(\frac{r_3}{r_2}\right)^2}\right)\left(\frac{{w_2}^2+{w_3}^2}{2VS_{01}^2}\right)\left(\frac{VS_{01}^2}{u_2^2}\right) \qquad (49).$$

When the results achieved from equations (48) and (49) are compared with those of literature, one must face the problem of lack of sufficient data for this kind of losses. However, comparing the values of the overall loss coefficient and efficiency with those reported in the literature, it seems that the above described correlations provide fairly reliable results.

4.2.5 Disk friction losses

Disk friction losses are produced in the enclosure between the back disk side of the impeller and the case of the machine, where an amount of fluid can leak due to the pressure gradient and rotate around the rotor axis.. In the present model, the formulation of Whitfield [13] was adopted, which is based on the original model of Daily & Nece [….], in alternative to the model proposed by Benson which provides exceedingly large values with respect to the available test data:

$$\Delta q_{R,df} = \frac{0.25\overline{\rho}\,u_{t,le}{r_2}^2 K_v}{\dot{m}} \qquad (50)$$

where:

$$k_v = \begin{cases} \frac{\left[3.7\left(\frac{\varepsilon_{ax}}{r_2}\right)^{0.1}\right]}{Re^{0.5}} & ,Re < 3\cdot 10^5 \\ \frac{\left[0.102\left(\frac{\varepsilon_{ax}}{r_2}\right)^{0.1}\right]}{Re^{0.2}} & ,Re > 3\cdot 10^5 \end{cases} \qquad (51)$$

$$Re = \frac{u_2 r_2}{v_2} \qquad (52).$$

As a possible alternative, providing similar results (in the range of 1%), the correlations proposed by NASA [14, 17, 18] can be recommended.

4.3 Diffuser loss

A diffuser is generally present in radial turboexpanders downstream of the rotor, in order to allow the partial recovery of the large kinetic energy still available through controlled diffusion of the fluid. The calculation of the diffuser loss follows the standard procedure described in [42].

5. Results and parametric analysis (Design process)

Making use of the above-described loss correlations, a parametric analysis has been run to assess the behavior of losses against the main design parameters and input data:

a. Blade height – inlet rotordiameter ratio (b_2/d_2)

b. *Flow coefficient (Φ)*

c. *Load coefficient (Ψ)*

d. *Isentropic degree of reaction (R_s)*

The reference case is a 50 kW turboexpander operating with a saturated or superheated vapour ORC between the upper/lower temperature levels of 147/95 °C (referred to R134a [37]).

5.1Blade height – inlet rotor diameter ratio (b_2/d_2)

This parameter influences the power output, mass flow rate, efficiency, blade shape and flow conditions, especially at rotor outlet (figures 6,7) for both radial (IFR) and backswept (IFG) rotor geometries. The mass flowrate (and thus the power output) increases linearly when b_2/d_2 is augmented. The absolute value is strongly dependent on the considered fluid: for example, the cyclohexane flow rate is much lower than that of the other working fluids, because of the larger specific enthalpy drop. Among the fluids here considered, R1234yf shows the highest flowrate. Generally, with the reduction of density and velocity of fluids, the required blade height ratio increases at fixed expander power output. It is also important to remark that, for a fixed flowrate, expanders with backswept blades (IFG) require higher

b_2/d_2 to achieve the same flow rate as for the IFR design Generally, the rotor outlet blade height increases with increasing b_2/d_2 (i.e. the ratio between hub and shroud diameters at rotor outlet, d_{3h}/d_{3s} decreases, figure 7). R134a and R1234yf show a particular trend, with remarkable differences between IFR and IFG designs (figure 7). This is due to the fact that the outlet rotor blade height is determined from the mass flowrate balance, with the constraint of axial flow. Consequently, the meridional component of the outlet rotor velocity increases with the reduction of blade height. Figure 7 reflects a widely different design geometry of expanders working with different fluids.)

a. 5.2Flow coefficient (Φ)

Φ defines the velocity triangle at impeller inlet. The flow coefficient is one of the main parameters in the design of turboexpanders, as it directly influences the mass flow rate, the performance (power output and efficiency), the geometry and the rotor number of blades. To give an idea of how Φ influences the flow, the variation of shape of the velocity triangle at rotor inlet at two different values of Φ is shown on figures 8 a) (radial rotor blades IFR) and 8 b) (backswept rotor blades IFG). Keeping constant the other non-dimensional design parameters,, the meridional component of the inlet absolute velocity (c_{m2}) increases with increasing Φ, whereas the peripheral velocity remains almost unchanged, as it mainly depends on the load coefficient. This results in an increase of absolute and relative velocity at rotor inlet (c_2 and w_2 respectively) and in a reduction of the related flow angles (α_2 and β_2). The change in β_2 directly affects the incidence losses, whereas α_2 influences the number of rotor blades, according to equations (13) and (14): as α_2 decreases with increasing flow coefficient, the number of rotor blades is reduced, as shown on figure 9 which reports the optimized values of Z_R vs. Φ. It must be remarked that, given the small size of the investigated expanders, it is a good practice trying to reduce large numbers of blades which results from the application of Eq. 14 (Glassman theory), in order to reduce the blockage effects. In fact, it is still possible to achieve high efficiencies also with a number of rotor blades much lower than that proposed by Eq. 14. Within the considered field of flow coefficient (typical of radial turboexpanders, $0{,}08 < \Phi < 0{,}22$) , no significant differences in the "optimal" number of blades was found for the different investigated fluids (R134a shows the lowest optimal number of blades, whereas CycloHexane shows the highest one, for both IFR and IFG geometries).From figure 10, it is evident that backswept bladed (IFG) expanders have a total to static efficiency (η_{ts}) 1.5 – 2 points higher than radial (IFR) ones, which is in agreement with [18]. Generally, η_{ts} increases with Φ (with the exception of

cyclohexane for IFG rotors). The highest values of η_{ts} are achieved by R134a and R1234yf, whereas the lowest ones are shown by R245fa and cyclohexane.

5.3 Load coefficient (Ψ)

Ψ is a fundamental parameter in the design of turboexpanders, because it deeply influences their performance (rotational speed, absolute and relative flow angles at nozzle outlet/rotor inlet, overall performance) and is, with the degree of reaction, one of the main non dimensional parameters to define the different categories of rotors. Keeping constant the other non-dimensional design parameters (table 1), an increase in the load coefficient leads to a reduction of the meridional component of the absolute velocity at rotor inlet (see modification of velocity triangles in figure 11). Thus, the mass flow rate is reduced and its effect is added to the reduction of the expander total enthalpy drop, leading to an overall reduction of power output. Due to the reduction of the meridional and peripheral velocity at rotor inlet, the absolute angle α_2 increases, which implies a reduction of the relative velocity (w_2'). For this reason, the load coefficient has a large influence on the incidence angle and on the associated loss. Figure 11 shows how the optimized velocity triangle for IFR tends to that of IFG with increasing Ψ. The trend of the rotational speed vs. load coefficient is shown on figure 12. It is interesting to remark the difference in rotational speed with different working fluids, which is in turn related to thetotal enthalpy drop and to the rotor size. Specifically, the largest rotational speeds occur for R134a and R245fa, whereas those of CycloHexane are considerably lower. Generally, a backswept (IFG) design allows a lower rotational speed. The dependence of the nozzle outlet/rotor inlet absolute velocity angle (α_2) on the Load Coefficient Ψ is shown on figure 13. These expanders are characterized by large nozzle flow angles, which become even higher in case of backswept blades. The largest values of α_2 for rotors with radial blades (IFR) are reached by CycloHexane and by R1234yf and R245f in the case of an IFG design . In both IFR and IFG configurations, R134a shows the lowest values of α_2. The trend of the relative velocity angles at rotor inlet (β_2) vs. Ψ is shown on figure 14. The highest absolute values are shown by cyclohexane and R1234yf for radial bladed rotors and R245fa and R1234yf for the backswept bladed ones. Anyway, when Ψ is within the range 1.05 – 1.15, β_2 values are at the same levels for the different fluids in the case of backswept bladed rotors (IFG).

5.4 Isentropic degree of reaction (R_s)

R_s is defined as the ratio between the static isentropic enthalpy drop through the rotor and that of the overall stage. It strongly affects the performance of the expander.When combined with the other main parameters Φ and Ψ, it completes the definition of the

design geometry. When the other design parameters are fixed, with increasing R_s the isentropic stator static enthalpy drop is reduced. For this reason, the pressure at the stator outlet is higher and the related fluid density is increased. With fixed stator outlet cross sectional area, given the relatively limited change in mass flow rate, the meridional component of the absolute velocity is reduced, which offsets the increase in static pressure. Keeping constant the flow coefficient, the rotational speed is reduced. The related velocity triangle is modified as shown in figure 15. The expander power output decreases with increasing R_s of an amount variable with the different investigated fluids, as shown in figure 16. R245fa is the least sensitive to R_s because it has the lowest flowrate level and thus the lowest reduction of power output. Moreover, IFR expanders with radial blades have higher R_s than those with backswept blades. The variation of R_s has strong effects on the rotor peripheral speed. Referring to figure 17, the remarkable difference in peripheral speed for the different investigated fluids and rotors can be noticed. Specifically, R245fa shows the highest values, whereas the lowest is shown by R1234yf, due to its low value of the total enthalpy drop. Finally, the backswept rotors (IFG) have a lower peripheral speed compared to the radial bladed ones. This is due to the higher load coefficient Ψ (with fixed total enthalpy drop) which characterizes the backswept geometry.

6. Interpretation of results - Design process

6.1 IFR vs IFG design

Moving from the radial (IFR) to backswept blades (IFG) configuration, the load coefficient increases Thus, in the backswept (IFG) design the meridional component of velocity at rotor inlet is reduced to maintain the fixed flow coefficient. For this reason, in order to achieve the target 50 kW power output, the IFG design shows higher b_2/d_2 ratios. An additional consequence of the higher load coefficient of backswept bladed rotors is their lower peripheral velocity (and rotational speed) for a given rotor size. Finally, backswept machines show a lower degree of reaction than the corresponding radial bladed ones. As remarked in the parametric analysis, when the overall enthalpy drop (stator + rotor) is fixed, the reduction of the degree of reaction implies a lower stator outlet backpressure and, consequently, a lower fluid density in this section. As the outlet conditions are fixed, and because the mass flowrate undergoes only limited variations, the meridional component of the absolute velocity increases to counterbalance the reduction of fluid density. Thus,

in order to maintain the flow coefficient unchanged, the peripheral velocity at rotor inlet increases. Finally, in order to keep the load coefficient constant, the total enthalpy drop of the expander is increased and, consequently, the related power output. In this way, by tuning b_2/d_2, the load coefficient and the reaction degree, it is possible to move across the two different configurations. Generally, backswept bladed expanders show 1.5 – 2% better efficiency levels than the corresponding radial bladed ones.

6.2 Different working fluids

A specific interpretation of the results is needed when considering the important matter of expander design with different working fluids. All those here considered are good candidates for the power cycle specifications (power output, temperature levels). On the other hand, large differences in kinematic, geometric and performance characteristics are found between the different fluids. In the following figures, the behavior of R134a, R1234yf, R245fa and cyclohexane is extensively reported. Anyhow, for sake of completeness, the analysis of different fluids has been extended to R236fa and CycloPenthane. The inlet diameter of the expander is in the range 80 – 110 mm. The largest size were achieved for the hydrocarbons like cyclohexane and N-Pentane, due to their much lower density, in spite of the larger specific isentropic enthalpy drop compared to HFCs. The rotational speed is between 30000 and 50000 rpm, generally lower for backswept configurations due to the lower peripheral velocity (see the generic shape of velocity triangles in figure 15). Among the different fluids, the cyclohexane shows the lowest rotational speed, due to the much higher diameter, in spite of the high peripheral speed. The specific speed is in the 0.055 – 0.1 range. The highest value is shown by the cyclohexane because, in spite of the lowest rotational speed and the highest stage enthalpy drop, they are largely counterbalanced by the very high values of volumetric flowrate due to the lowest density. The flow at nozzle exit is generally supersonic ($0.9 < M < 1.5$), with the exception of R1234yf due to the high values of blade height at section 2 (b_2, table 3). The highest value of Mach is shown by CycloHexane, due to the combined effects of low density and high peripheral speed. Generally, high nozzle exit angles are found (77 – 83.5 °), with larger values for backswept rotor (IFG) design. When considering the flow within the rotor, a high deflection level has to be remarked, which is in the range 40 – 90°, generally higher for backswept configurations. Due to the shape of velocity triangles (see velocities and angles on table 3), cyclohexane shows the highest deflection level for the IFG configurations and the lowest for the IFR ones. The hub to tip diameter ratio at rotor exit (d_{3h}/d_{3s}) is in the 0.39 – 0.52 range and agrees with literature data [14, 17]. At rotor exit, the adoption of a diffuser for the partial recuperation of the kinetic energy may be important only for fluids like cyclohexane, which have high values of

519 absolute Mach number in this section. The total- to-total efficiency of the investigated expanders
520 and fluids ranges between 0.72 and 0.80, generally higher for backswept configurations than for the
521 corresponding radial ones. Generally, higher efficiencies are achieved with expanders having lower
522 velocities and deflections. Finally, it is important to remark that, for the specific size here
523 considered (50 kW), sub-atmospheric values of total pressure at rotor exit are not recommendable.
524 Thus, CycloHexane and pentane are critical from this point of view, in spite of their interesting
525 efficiency levels in ORC. On the basis of expander design and cycle performance, R245fa and
526 R236fa represent thus the most interesting options.

527 **6.3 Distribution of losses and efficiency**

528 It is also important to analyze the distribution of the different losses through the expander, whose
529 contribution to the overall reduction of efficiency ($\Delta\eta$) is shown in table 3. It is practically the same
530 for the different investigated fluids and configurations. The contribution of the *stator losses* to the
531 overall losses ranges between 2% of R134a and 12% of cyclohexane, both referred to radial
532 geometry. Especially in IFR configurations, the stator losses have the highest incidence for
533 hydrocarbons (mainly cyclohexane) and R245fa compared to the other investigated fluids. It is
534 mainly due to the high velocity in the nozzle (table 3, see also the high values of M_2). Literature
535 data [13] report that the *stator losses* generally range between 5 and 15% of the overall, which is in
536 line with the results achieved with the here proposed model.

537 Under design conditions, the *incidence losses* are negligible, as the relative velocity angle at rotor
538 inlet is the optimizing value calculated by the (15 – 17) and (21) relationships. Their contribution to
539 the overall reduction of efficiency $\Delta\eta_{ts,i}$ ranges between 0.03 and 0.2%.

540 The *disk friction losses* give a contribution within the 2 – 4% to the total and have a reduced relative
541 influence on the expander efficiency (0.4 % $<\Delta\eta_{ts,v}<$ 0.8 %). The highest values are shown by the
542 cyclohexane, mainly due to the large rotor diameter and peripheral velocity.

543 The *tip clearance* losses, here referred to an average 3% clearance fraction of blade height and to
544 backswept configuration, give a relevant contribution on the total losses, ranging from 10% of
545 R1234yf to 21% of CycloHexane. Generally, higher tip clearance losses are shown by fluids having
546 higher ratio between radial clearance and inlet blade height (ε/b_2), in agreement with eq. (43). The
547 related overall efficiency drop $(\Delta\eta_{ts,cl})$ is within the 2 - 6.5% range and agrees with literature data
548 [30, 39].

549 The highest relative contribution to the losses (60 – 70%) is given by *secondary flows* in the rotor,
550 which are due to the high blade curvature and pressure gradient through the blade vanes. As
551 suggested by Rodgers [40], this contribution is shared between blade loading and profile curvature.
552 The former represent the highest contribution to overall losses, ranging from 27% to about 50% of
553 total. The highest values are found for R134a and 1234yf, which have the lowest number of blades
554 and thus the highest blade loading. For this reason, cyclehexane shows the lowest relative
555 contribution of blade loading losses, in agreement with equation (48). Their contribution to the
556 efficiency reduction ($\Delta\eta_{ts,cp}$) is variable between 8 and 13 %.

557 The contribution of profile losses to the overall turbine losses ranges from 12% of R134a to 27% of
558 R1234yf. Their share on the overall losses is generally higher for hydrocarbons, ranging from 20 to
559 26%. It is attributable to the combined effects of rotor geometry (i.e. higher d_3/d_2), fluid properties
560 (i.e. sound speed) and kinematic conditions (i.e. higher relative velocities w_2 and w_3), in agreement
561 with eq. (49). They provide a total to static efficiency drop ($\Delta\eta_{ts,p}$) variable from 3 to more than
562 8%..

563 The *friction losses in the rotor* also represent an important contribution to the overall efficiency
564 drop, reducing its value ($\Delta\eta_{ts,a}$) from 0.9 to about 2.3 percentage points. They are generally higher
565 in cases of turbines with larger wet surface like, for example, cyclohexane.

566 Finally, it is also important to consider the *kinetic energy loss at expander output.*. Even though a
567 diffuser has always been considered here, this loss is representative of the difference between total
568 to total (η_{tt}) and total to static (η_{ts}) efficiency of the expander. On the whole, these losses are not
569 negligible, as they can reach up to 12% of the total. They are capable to reduce the overall
570 efficiency ($\Delta\eta_{ts,v}$**)** from 0.39 to 1.15 %. It is thus possible to recommend that a diffuser is always
571 included in the design of these expanders.

572 The comparison of the results with those achieved by Rohlik [14, 17, 20] shows a substantial
573 agreement, even though they were referred to air. Specifically, the highest contributions to the
574 overall efficiency drop are given by blade loading and profile losses into the rotor. A similar
575 behavior is found also for the remaining losses, even though the stator and disk friction losses
576 calculated in this model give a generally lower contribution compared to [17]. On the contrary, the
577 tip clearance losses are generally higher than those proposed by Rohlik [17]. Anyway, they are on
578 line with those originally proposed by NASA [30] and successively confirmed by numerical
579 calculations [39]. The comparison of the total to static efficiency of the here designed expanders
580 with those achieved by Rohlik in the maximum efficiency curve [30] and with the experimental

results from similar machines [24], shows a good agreement regarding the design specific speed, whereas lower values of the efficiency are achieved here, especially for radial bladed expanders (figure 18). This is mainly due to the different size, geometry and working fluids considered in the present investigation, as well as to the different relationships adopted for the calculation of losses. Finally, the comparison of the results achieved in this work with those coming from experimental campaigns of Benson [24] shows a complete agreement.

7. Off design performance prediction of the radial turbo-expander

The above discussed design procedure can be used to build the characteristic curves of the expanders, which fundamental to predict their off- design behavior. When dealing with ORC working partially or totally with not continuously available renewables, it often happens that they work most of time under off design conditions. It is the case, for example, of solar power stations or integrated geothermal – solar binary cycles, like those proposed in [10] and [36], where the variable amount of available solar heat leads to variable massflowrate and/or thermodynamic conditions of the produced organic steam at the turbine inlet. When the characteristic curves of the designed expanders are known, they can be used to provide an estimate of their performance under variable inlet conditions (off design) and - when possible- to adjust their rotational speed in order to minimize the losses.

Specifically, in this chapter we analyze the buildup of characteristic curves with variable temperature, pressure and fluid mass flowrate at the turbine inlet (the latter depends on pressure drop through the expander), for different values of the corrected speed:

$$N_c = \frac{N}{\sqrt{T_{01}}} \qquad (55)$$

In the off design approach, the turbine geometry is specified, resulting from the design procedure described in the previous sections. Specifically, the following geometric parameters are given as inputs:

- Blade height
- Stator and rotor inlet/outlet diameters
- Passage section areas
- Number of rotor and stator blades
- Blade metal angles

611 Moreover, in the present case the rotor outlet total pressure is maintained at the design value,
612 because it is fixed by the conditions at the condenser to satisfy the cogeneration conditions.
613 Anyway, with the developed model it is possible to let it be variable, in order to take into account of
614 the variable conditions at the condenser due to the timely change of the environmental conditions.

615 The loss correlations under off design conditions are the same adopted in the expander design, as
616 well as those relating flow and metal angles. These allow the determination of the actual flow
617 angles given the blade metal angles and the size of the expander, both coming from the design
618 procedure.

619 In order to analyze the off-design behavior of the turbo expander, the inlet total pressure and
620 temperature are changed. Consequently, the mass flowrate is determined from the inlet – outlet
621 pressure drop. Another possible way of estimating the off-design behavior is to fix the expander
622 inlet mass flowrate and total temperature and calculate the total pressure. Thus, the performance
623 maps of the expander (i.e. characteristic curves) are achieved by building the related curves under
624 design conditions for different values of N_c. They may be directly adopted within the
625 thermodynamic code for the analysis of the ORC. .

626 **7.1 – performance behavior at off design expander pressure ratio**

627 The curves of power output, mass flowrate and efficiency vs. off design pressure ratio at different
628 values of corrected speed N_c are shown on figures 19, 20 and 21 respectively, each one reporting
629 the results for both radial and backswept configurations. For the sake of brevity, the off design
630 analysis is carried out for R134a only, without losing in generality, as the behavior is qualitatively
631 similar for all the investigated fluids. From figure 19, it is clear that the power output is reduced
632 when the expansion ratio falls below the design value. Moreover, it is important to notice that the
633 power output is reduced with reducing the corrected speed: this is the result of the lower enthalpy
634 drop, due to the lower rotational speed, which is also responsible for the reduced variation of
635 peripheral velocity (i.e. the effective component for momentum). Finally, it should be remarked that
636 the reduction of power output with respect to the nominal value is larger than the reduction of the
637 pressure ratio, when N_C is at the design value: for example, when the expansion ratio is at 90% of
638 the design value, the power output is reduced to about 88% of the design value. When the
639 expansion ratio is at 80% of design value, the power output is about 75% of the nominal. The
640 overall behavior is found for both IFG and IFR geometries.

641

642 **7.2 – performance behavior at off design expander corrected mass flowrate**

643 The other typical turbomachinery off design parameter is the corrected mass flowrate, defined as

644 $$\dot{m}_c = \frac{\dot{m}\sqrt{T_{01}}}{p_{01}} \qquad (56).$$

645 Starting from the values of the total inlet pressure and temperature, from the maps of figure 20 it is
646 possible to determine the mass flow rate with variable expansion ratio for the different values of
647 the ratio $N_C/(N_C)_{des}$. It can be noticed that the radial bladed rotors (IFR) are more influenced by
648 operation under off-design pressure ratio than the backswept ones (IFG).

649 Figure 21 shows the behavior of total to static efficiency (expressed by the off-design to design
650 ratio) as a function of the variable (off-design) expansion ratio. It is important to remark the
651 relatively low sensitivity to the expansion ratio for corrected speeds below the design value, due to
652 the typical accelerating behavior of fluids into the expanders, which allows to work into a relatively
653 wide range of incidence angles with only a limited increase of loss coefficients. Hence, the
654 reduction of N_c below the design value could be regarded as a way to reduce the efficiency drop of
655 the expander at reduced values of the expansion ratio. As it is seen, the investigated expanders show
656 a relatively limited sensitivity of the efficiency to off design expansion ratio, unless it is reduced to
657 very low values. It is interesting to notice the increasing efficiency (1.5 – 2%) at corrected speed
658 lower than the design value. To better understand this behavior, it is important to analyze the
659 variability of velocity triangles under the three different values of corrected speed (figure 22), Let
660 us consider a reduction of corrected speed N_c at fixed thermodynamic conditions of the inlet fluid.
661 As the inlet – outlet expander pressure drop is fixed, the flow rate remains practically unchanged.
662 The lower variation of peripheral velocity leads to a reduction of stage and nozzle enthalpy drop
663 (notice that $R \neq 0$). For this reason, the pressure at nozzle exit is higher, which leads to an increase of
664 fluid density. As the mass flow rate is constant, the meridional component of absolute velocity
665 must be reduced, thus the related velocity triangle height decreases. When N_c is reduced, at fixed
666 total inlet temperature (T_{01}), the rotational speed of the expander decreases largely , and thus also
667 the rotor peripheral velocity. The latter entails an increase of relative flow angle at rotor inlet (β_2) in
668 the same direction (see the modified red and green triangles of figure 24). Hence, the shape of the
669 velocity triangles is modified towards the backswept configuration. This modification affects the
670 loss coefficients of the expander. Specifically, a reduction of N_c down to 60 – 65% of the design
671 value leads to an increase of the incidence losses and a reduction of the stator, friction and
672 secondary flow losses, as reported on figure 25. This effect is due to the change of velocity profiles
673 within the rotor vanes. Finally, it is interesting to analyze the behavior of the ratio of the off-design

to design total to static efficiency ($\eta_{ts}/(\eta_{ts})_{des}$) vs the corrected speed ratio ($N_c/(N_c)_{des}$), shown on figure 24 for both radial and backswept configurations, at fixed design inlet total pressure and temperature. In both cases, η_{ts} is maximized at values of $N_c/(N_c)_{des}$where the sum of losses is minimum.

8. Conclusions

The paper describes the features and analyzes the results of a zero dimensional model for the design of high efficiency small size ORC expanders. Two basic rotor blade geometries (radial IFR and backswept IFG) and six different possible organic working fluids (R134a, R1234yf, R236fa, R245fa, Ciclohexane, N-Penthane) have been analyzed and discussed. In all cases, the power output has been fixed at about 50 kW. The reference thermodynamic data for the specific application are taken from [36]. The relationships for the estimation of the expander losses, as well as the main design parameters, have been collected by an extensive investigation of models and experimental data available in literature for radial turbo-expanders. Generally, literature for radial expanders is much less rich than for axial turbines and, often, data and models are derived from these last and from centrifugal compressor applications, with limited adaptments. Moreover, these relationships and models are referred to ideal gases and Mach relationships, which is also the approach often applied in many CFD calculation codes. In the present work, the model applies the most recent, currently available, equations of state of the investigated real fluids expanding into the ORC turbine.

For the investigated fluids, , the rotor diameters are in the 80 – 110 mm range and the rotational speed is variable between 30000 and 50000 rpm (specific speed is always below 0.1). The only exception is CycloHexane, which needs higher rotor diameters (190 – 200 mm) and a lower rotational speed. The designed expanders are mostly supersonic and have high values of nozzle exit angles (α_2=77 – 83.5 °), whereas the deflection of flow in the rotor is between 40 and 90 °. The outlet rotor hub to tip diameter ratio resulting from the developed calculation code is within the 0.39 – 0.52 range, which agrees with literature data. In order to partially recover the outlet kinetic energy of flow, the adoption of a diffuser at rotor outlet is proposed, which is particularly recommendable for the expansion of the cyclohexane, which has the highest value of Mach at rotor discharge.

The expected total-to-total efficiency of the designed units ranges between 0.72 and 0.80, depending on the considered fluid and geometry configuration. The highest contribution to the

expander efficiency losses is given by the secondary flows within the rotor (blade loading and profile curvature), due to the high curvature of blade profiles and the high pressure gradient.

The investigation, on the basis of overall thermodynamic, power plant and fluid dynamic features, shows that the most suitable fluids are R236fa and R245fa, followed by R134a and R1234yf, whereas the worst ones are CycloHexane and CycloPenthane, which are further penalized by the sub atmospheric pressure at the expander output.

Generally, backswept bladed rotors (IFG) show 1.5 to 2.5% higher efficiencies. Moreover, they have larger values of the number of blades, load coefficient, nozzle exit angle and rotor deflection angle than the corresponding radial bladed ones. The peripheral speed and the reaction degree of the backswept configurations are instead lower. Generally, the results of the design and parametric analysis are in agreement with literature dataThe proposed calculation model has been successively used to predict the off- design performance, through the construction of the expander characteristic curves (corrected mass flowrate, power output and efficiency as functions of expansion ratio and corrected speed N_c). These last can be directly introduced into the thermodynamic ORC calculation code to evaluate the off design behavior of the expander under variable thermodynamic inlet conditions (total temperature and pressure and mass flow rate for different values of corrected speed), once the geometry of the expander is defined.

The calculation tool is open to improvements by the use of 2D – 3D CFD models and experimental tests on existing rotors, which potentially could allow the improvement of the less convalidated correlations, making it effective and reliable for the design and off-design analysis of radial turbo-expanders for small-size ORC powerplants.

List of figures

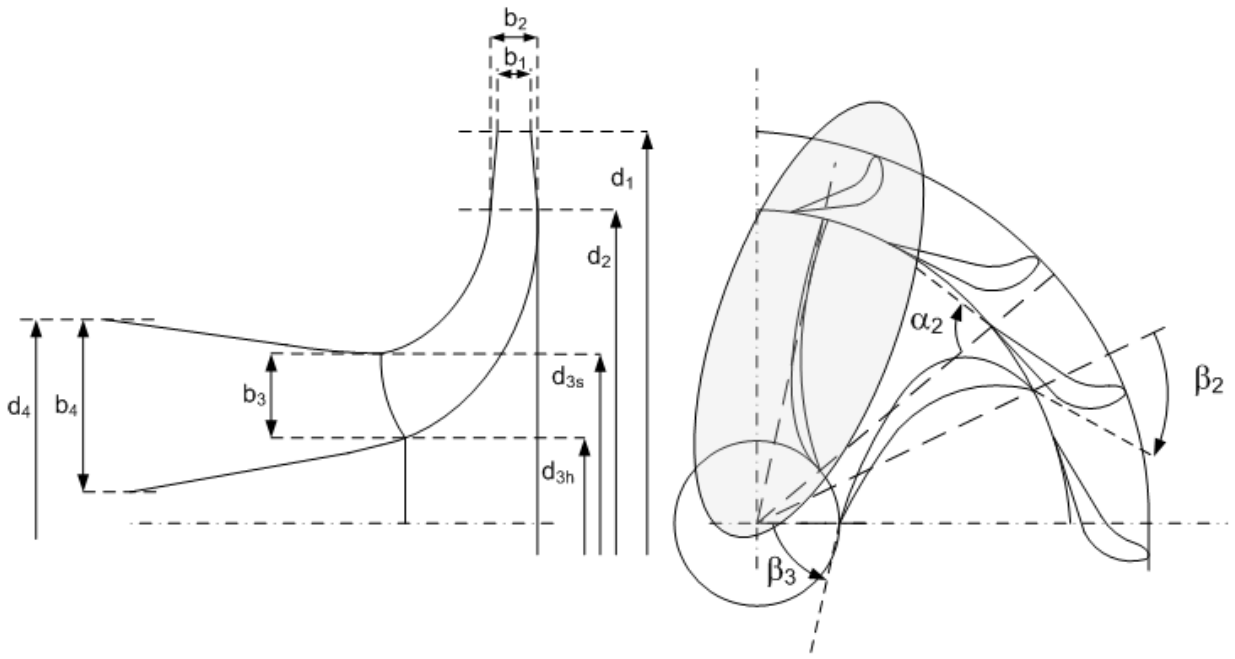

Figure 1 – General schematic of Radial inflow turbine: 90° IFR (shaded), and General rotor shape (IFG, unshaded).

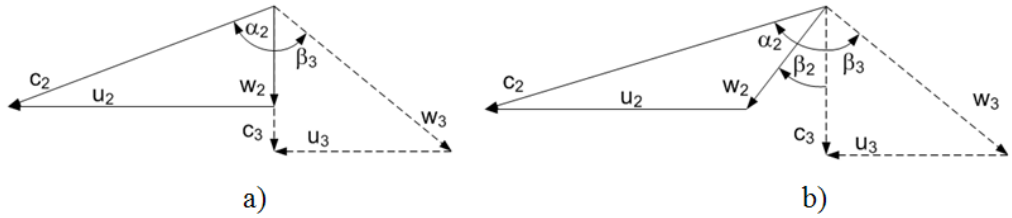

Figure 2 – Velocity triangles – nominal conditions; (a) 90° IFR (b) General (IFG)

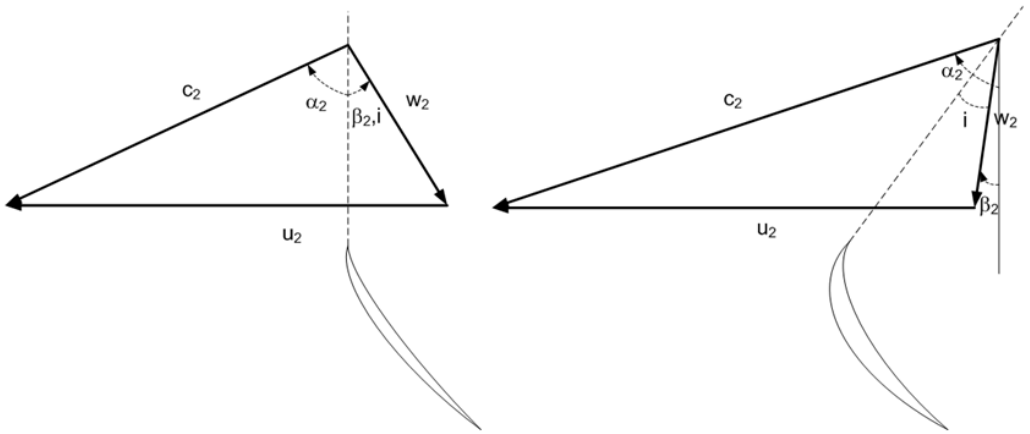

Figure 3 – Velocity triangles – optimal incidence conditions; (a) 90° IFR (b) IFG

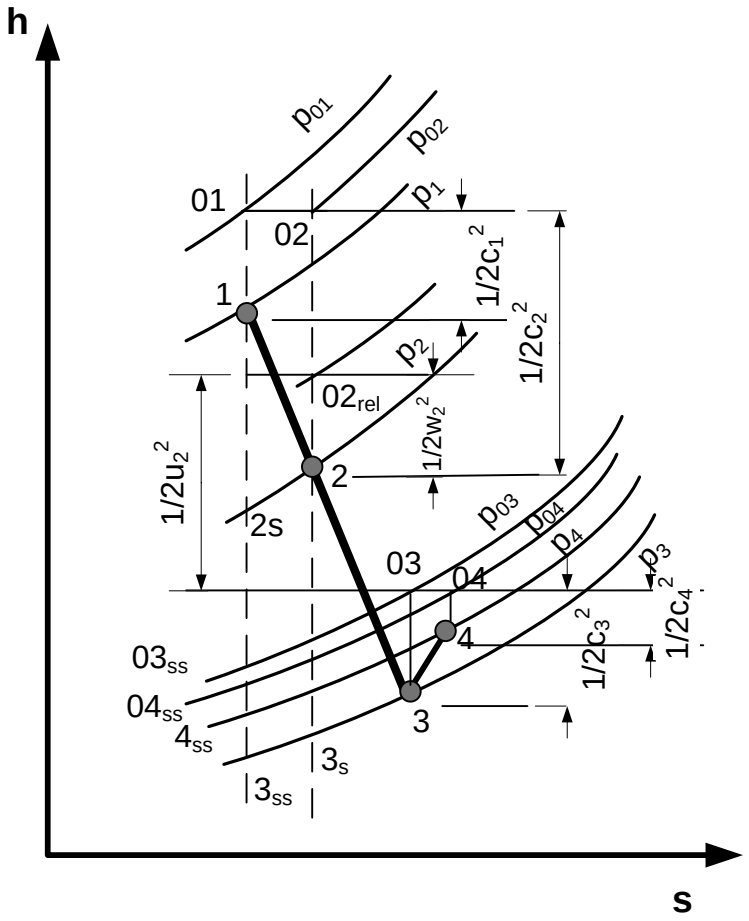

Figure 4: Enthalpy – Entropy representation of the expansion process [14].

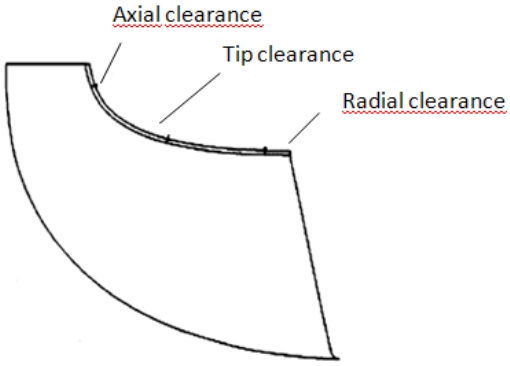

766

767 *Figure 5: Tip clearance along the development of a rotor blade.*

768

769

770

771

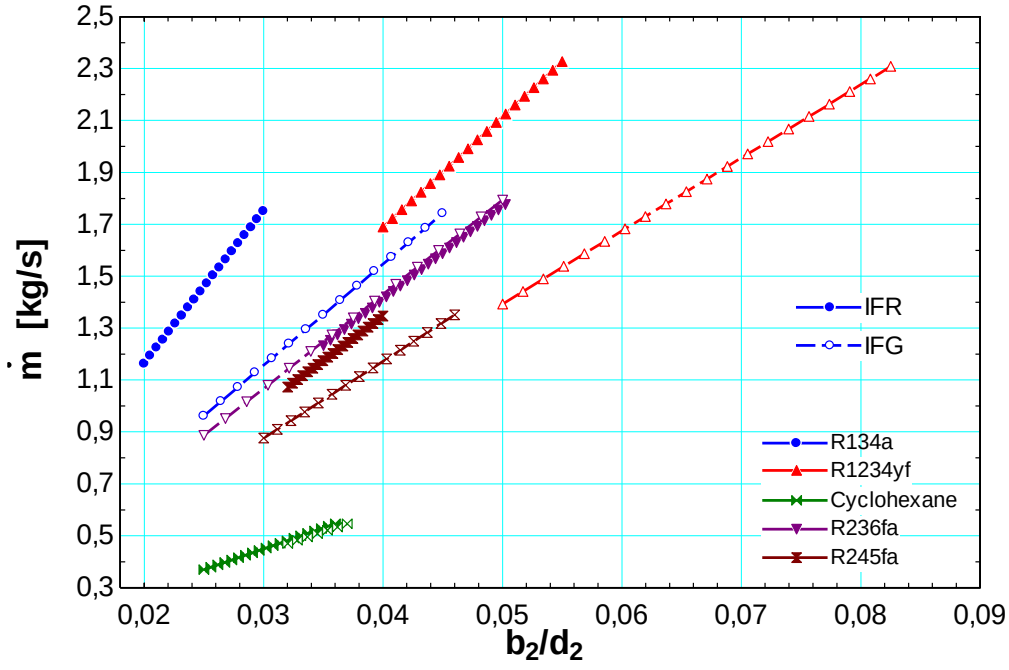

772

773

774 *Figure 6: mass flow rate and ratio of rotor exit diameter at hub and shroud as a function of ratio*

775 *between blade height and diameter at rotor inlet b_2/d_2 (IFR and IFG)*

776

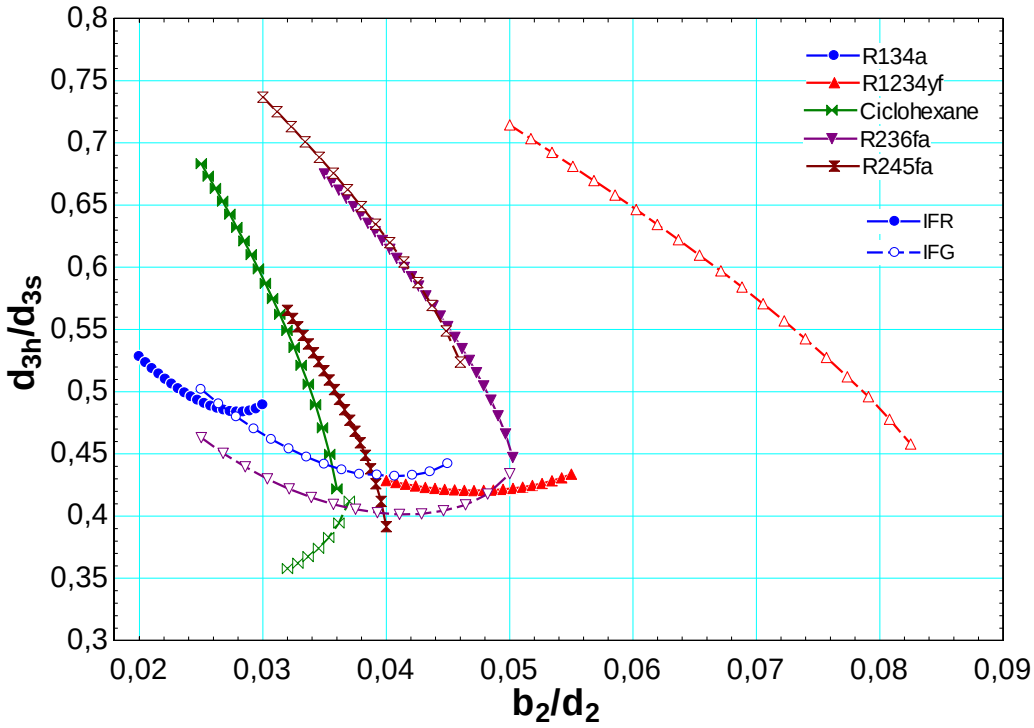

777

778

779 *Figure 7: Mass flow rate and ratio of rotor exit diameter at hub and shroud as a function of ratio*

780 *between blade height and diameter at rotor inlet b_2/d_2 (IFR and IFG)*

781

782

783

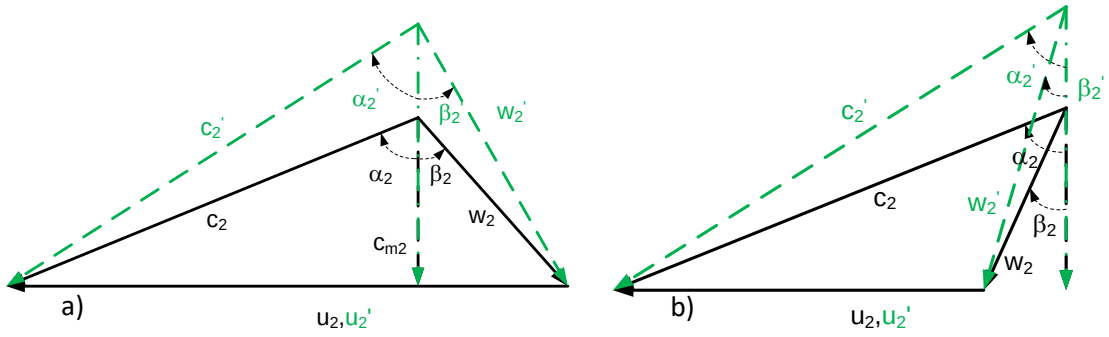

784

785

786 *Figure 8: Variation of velocity triangles with increasing flow coefficient*

787 *(from solid black to dashed green, a) IFR, b) IFG)*

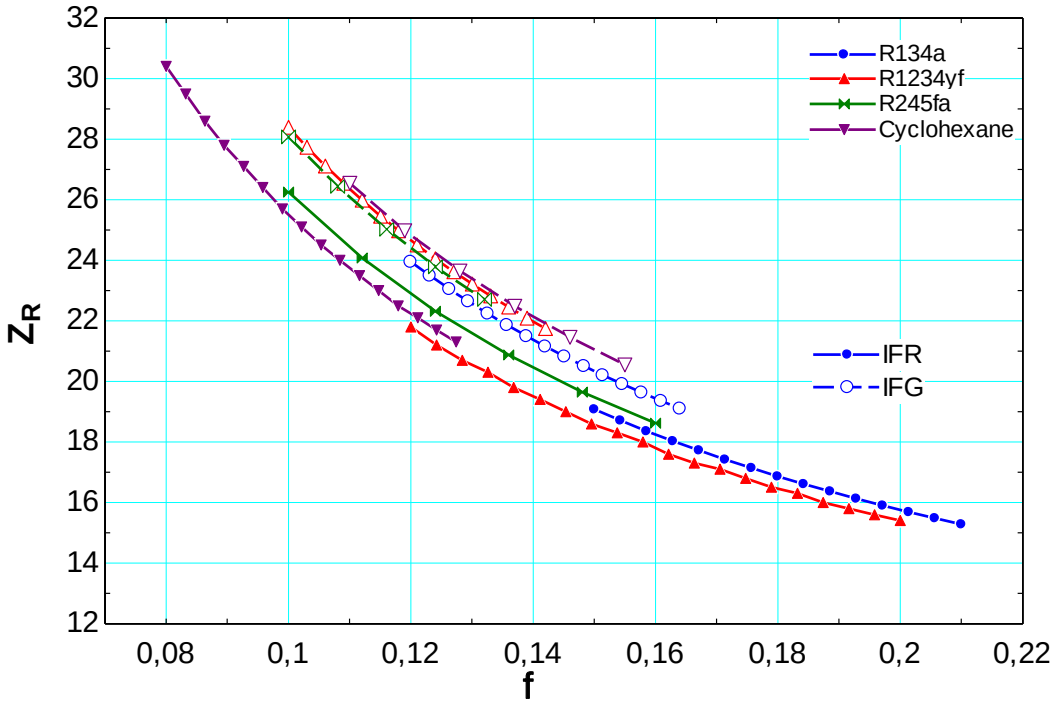

Figure 9: Number of rotor blades as a funcion of flow coefficient (IFR and IFG)

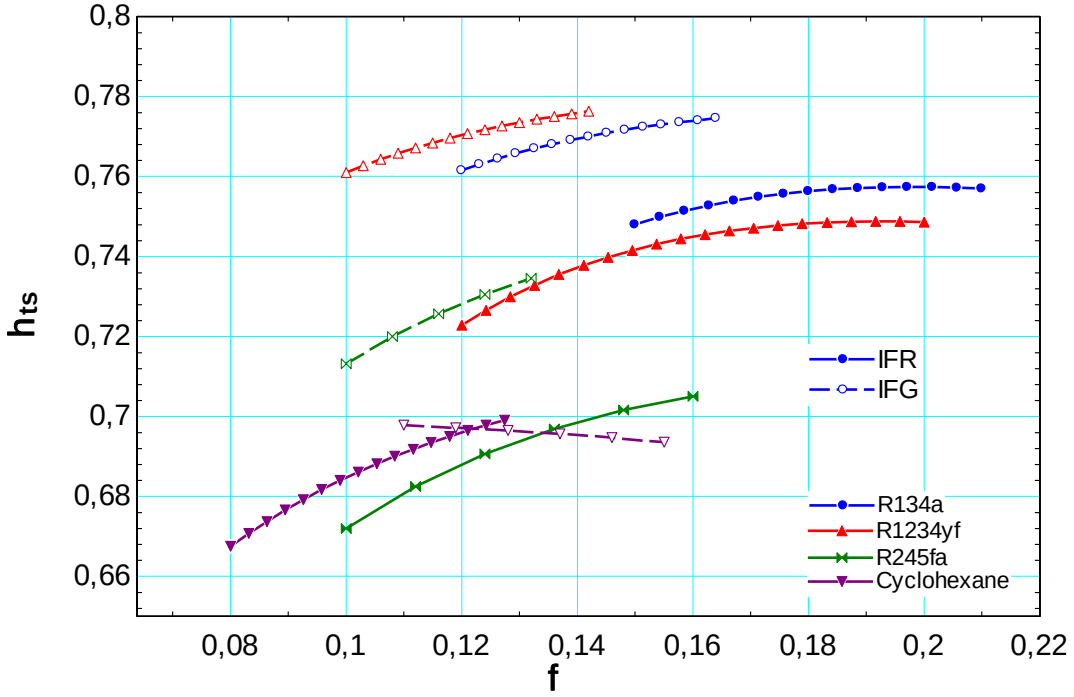

Figure 10 –Total-to-static efficiency as a funcion of flow coefficient (IFR and IFG)

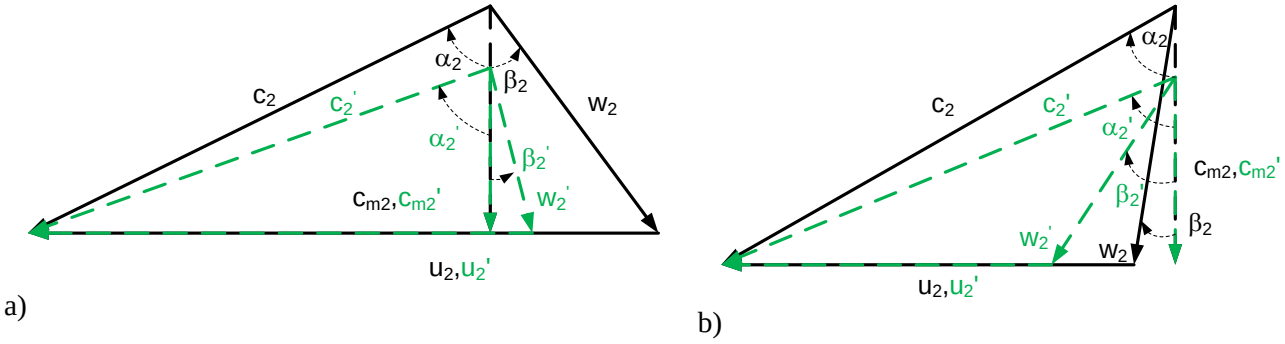

Figure 11 – Variation of velocity triangles at rotor inlet with increasing load coefficient (from black solid to green dashed) a): IFR; b) IFG

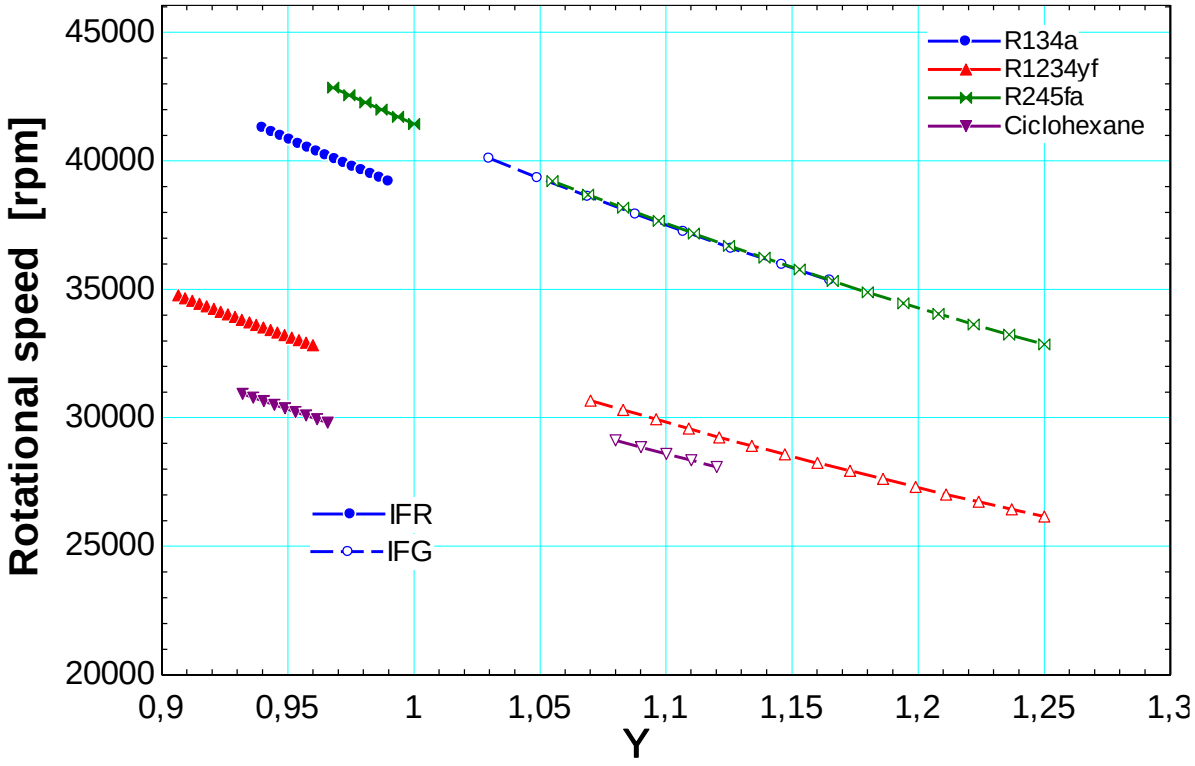

Figure 12: Speed of revolution vs. load coefficient (IFR and IFG)

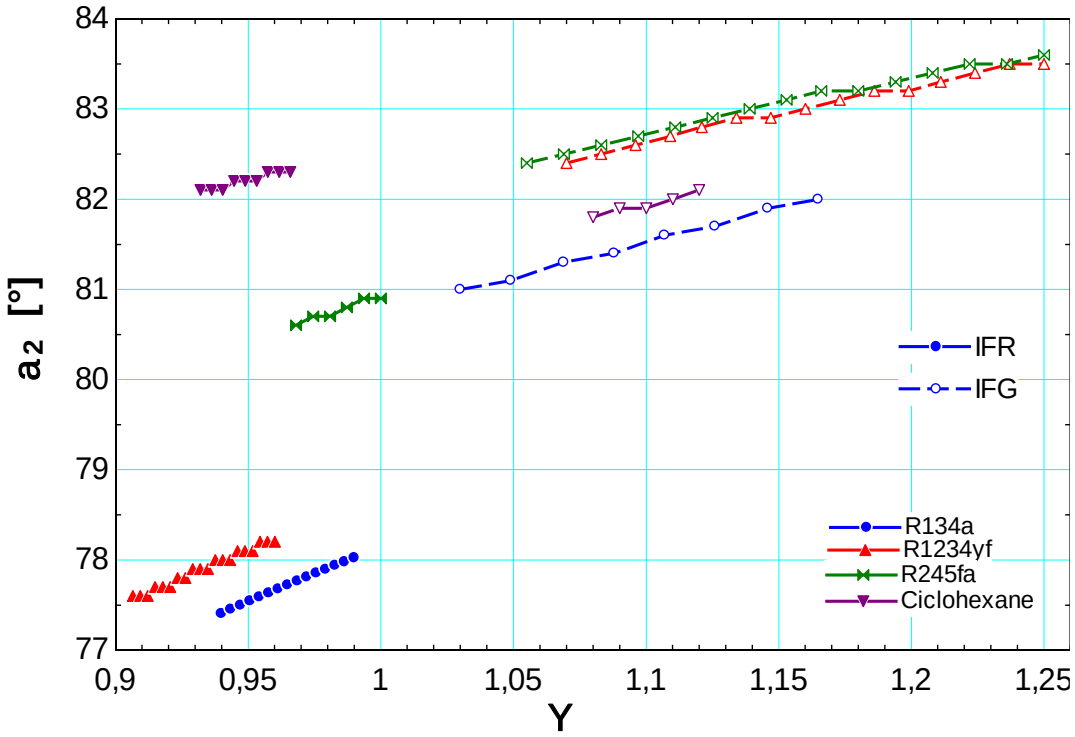

Figure 13 –Angleof absolute flow velocity (α_2) at nozzle outlet/rotor inlet vs. load coefficient (IFR and IFG)

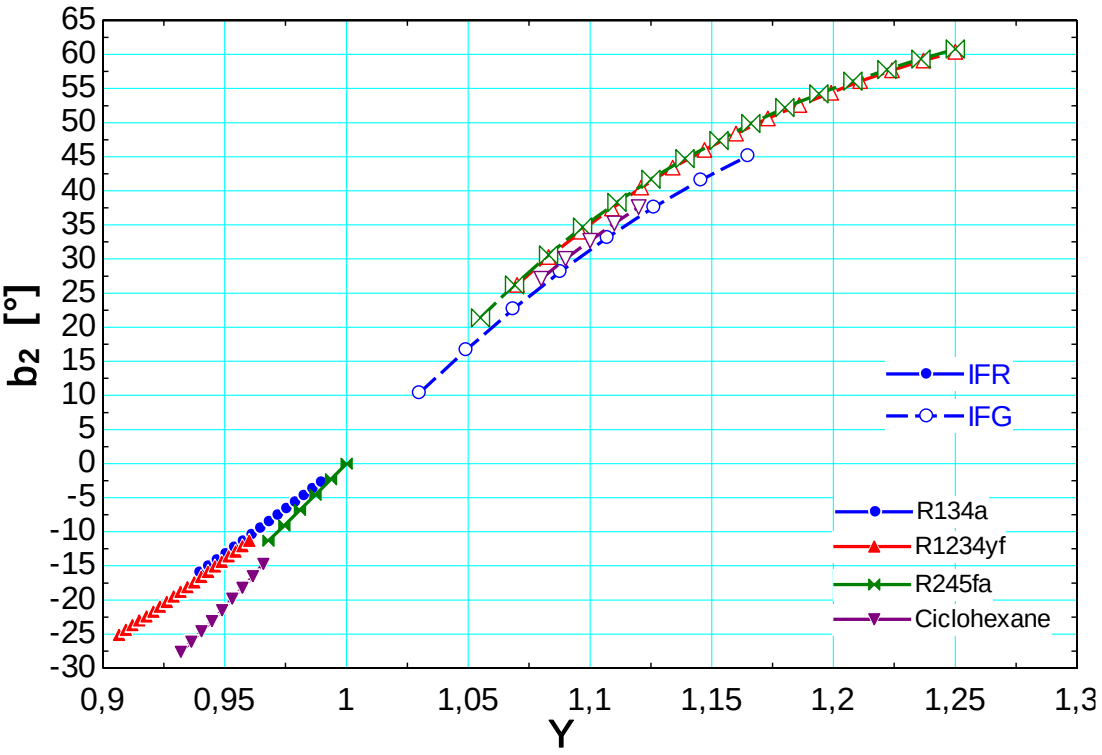

Figure 14 –Angle of relative flow velocity (β_2) at nozzle outlet/rotor inlet vs. load coefficient (IFR and IFG)

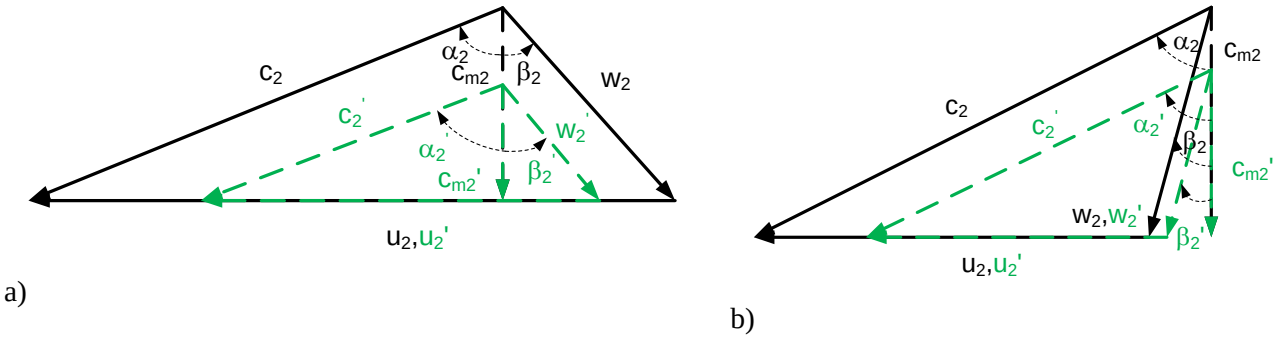

Figure 15: Variation of velocity triangles with increasing in isentropic degree of reaction R_s (from black to green, a) IFR, b) IFG)

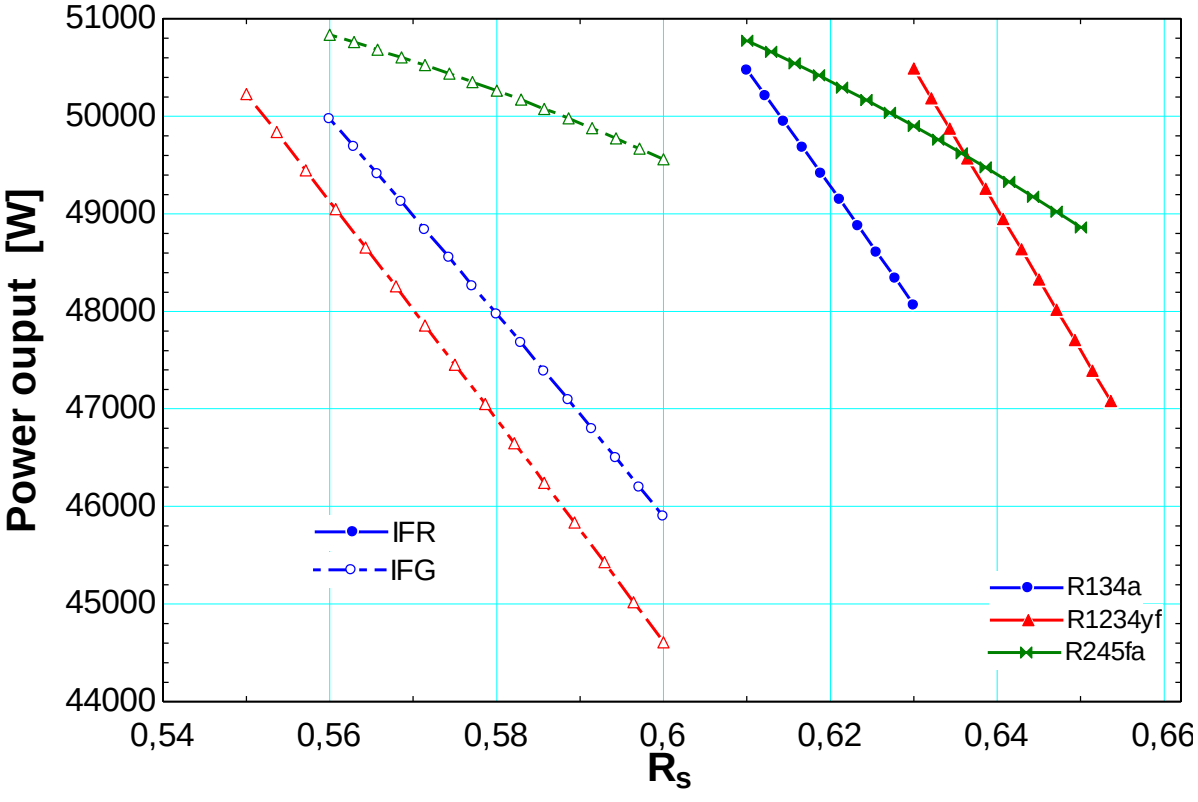

Figure 16: Expander Power output vs. isentropic degree of reaction (IFR and IFG)

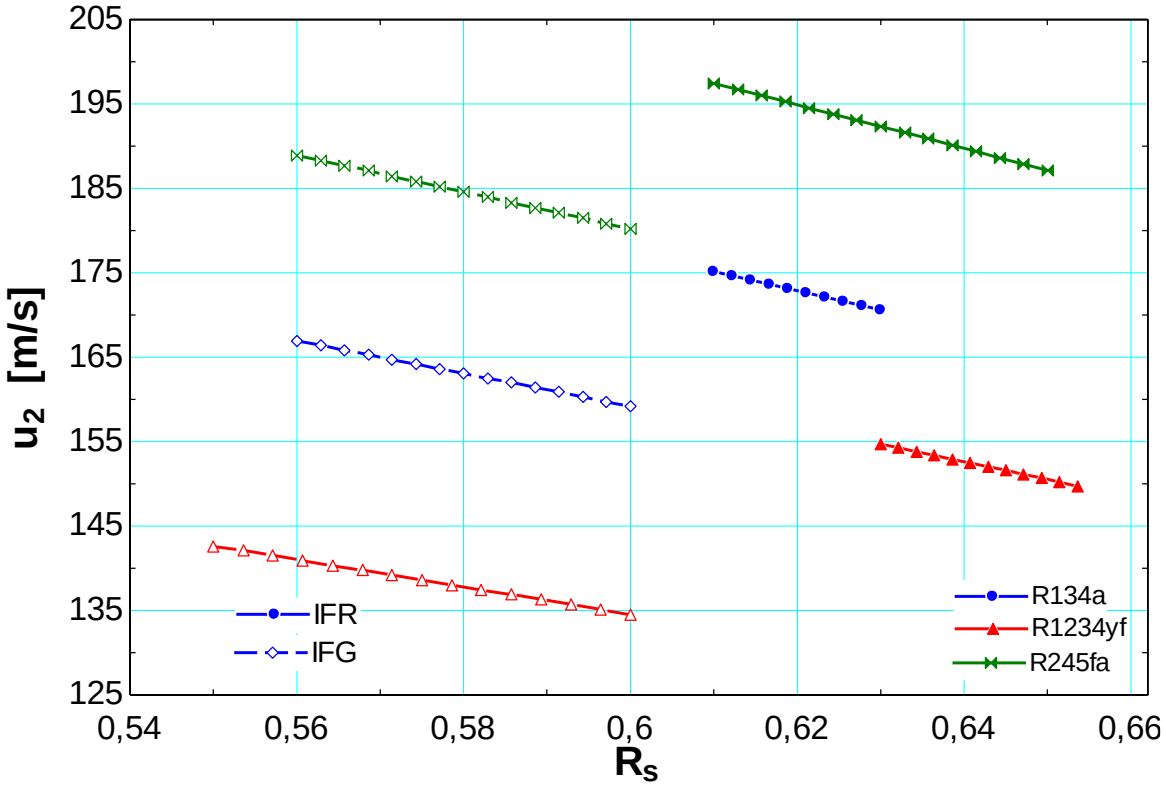

Figure 17: Expander peripheral velocity at rotor inlet vs. isentropic degree of reaction (IFR and IFG)

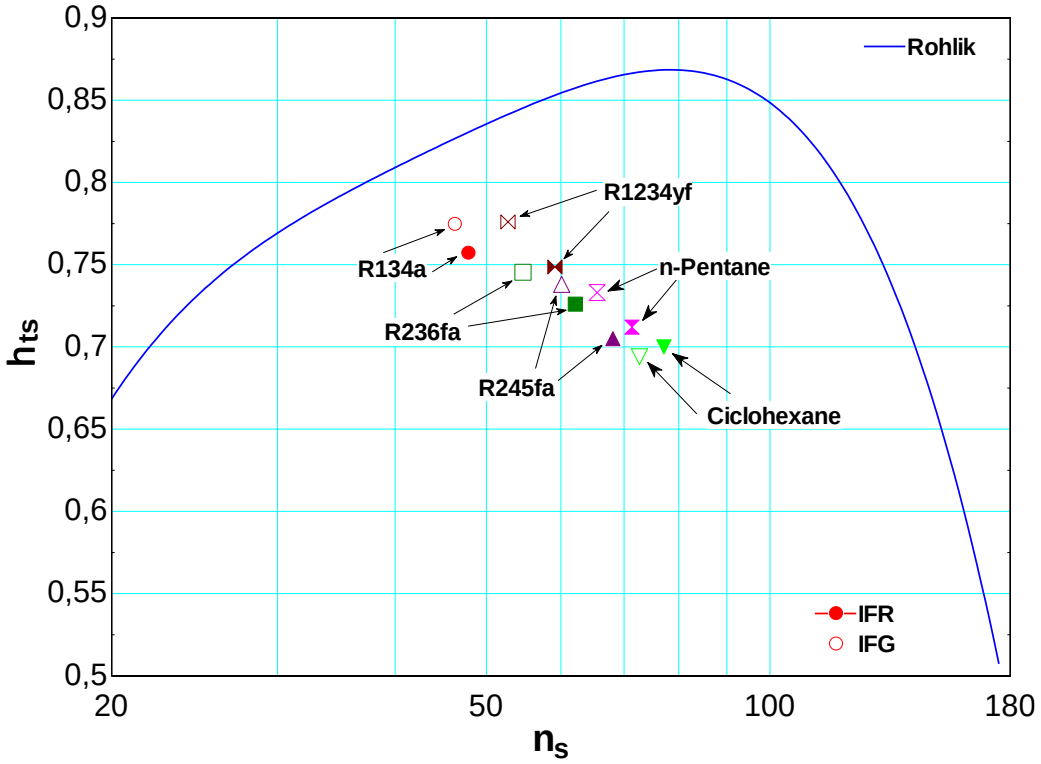

Figure 18: comparison of total to static efficiency of the here designed models with the results of Rohlik [30] (IFR and IFG)

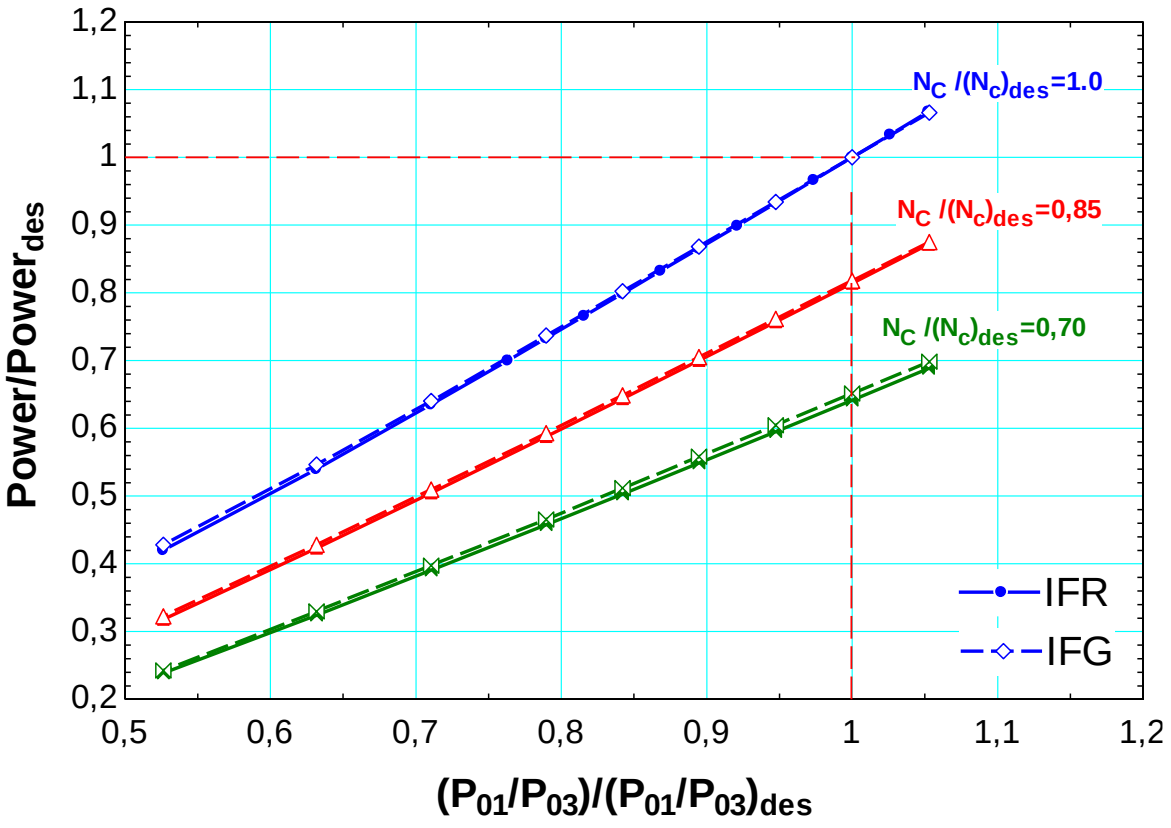

Figure 19 – Power output ratio – expansion ratio characteristic curve of the expander (Referred to R134a)

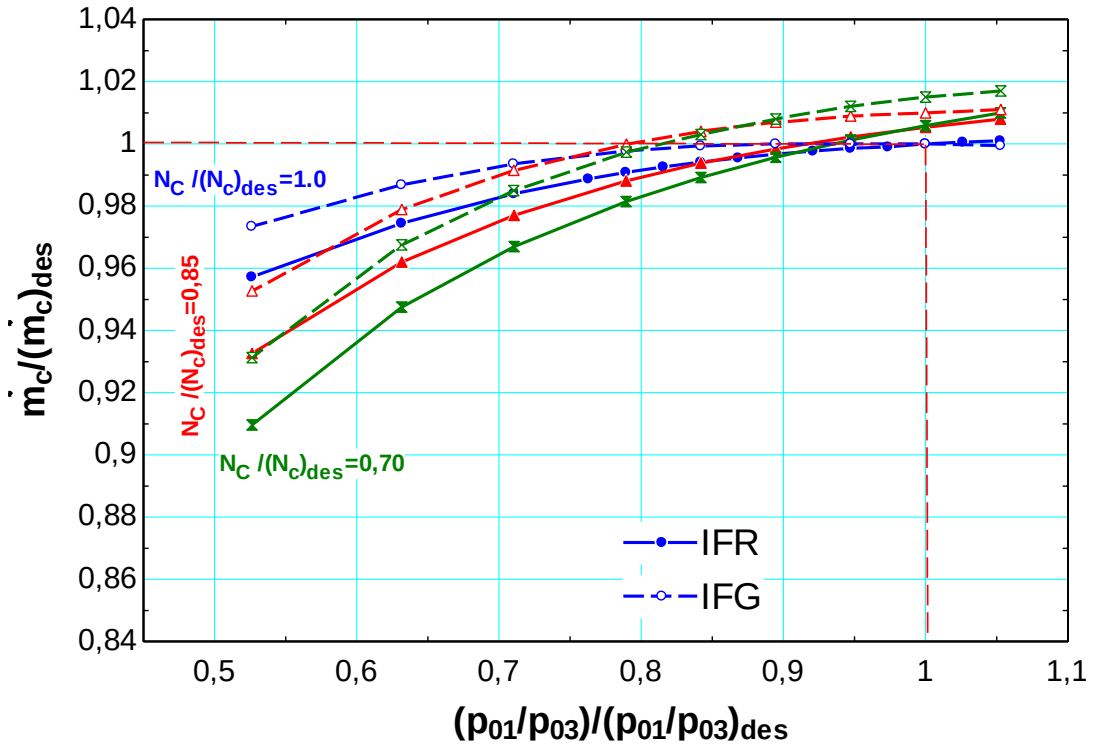

833

834 *Figure 20 – Corrected flow rate – expansion ratio characteristic curves of the expander (Referred*

835 *to R134a)*

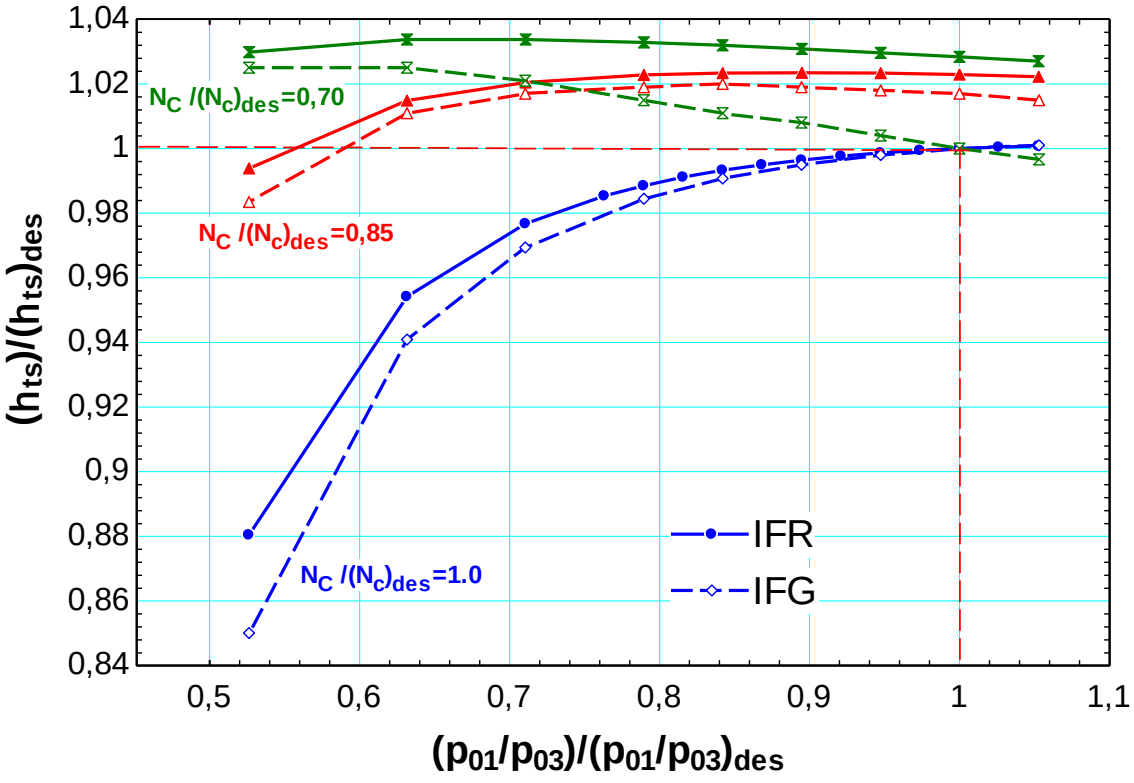

836

837 *Figure 21 – Total to static – expansion ratio characteristic curves of the expander (Referred to*

838 *R134a)*

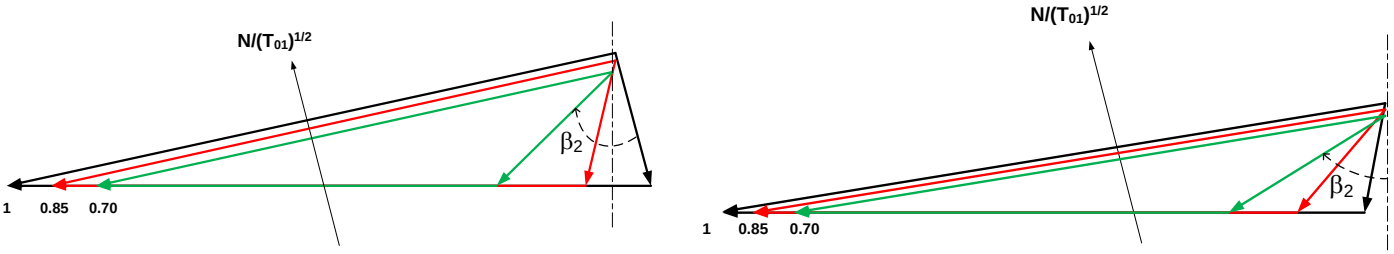

a) Radial blades *b) Backswept blades*

Figure 22 – Velocity triangles at rotor inlet at variable corrected speed

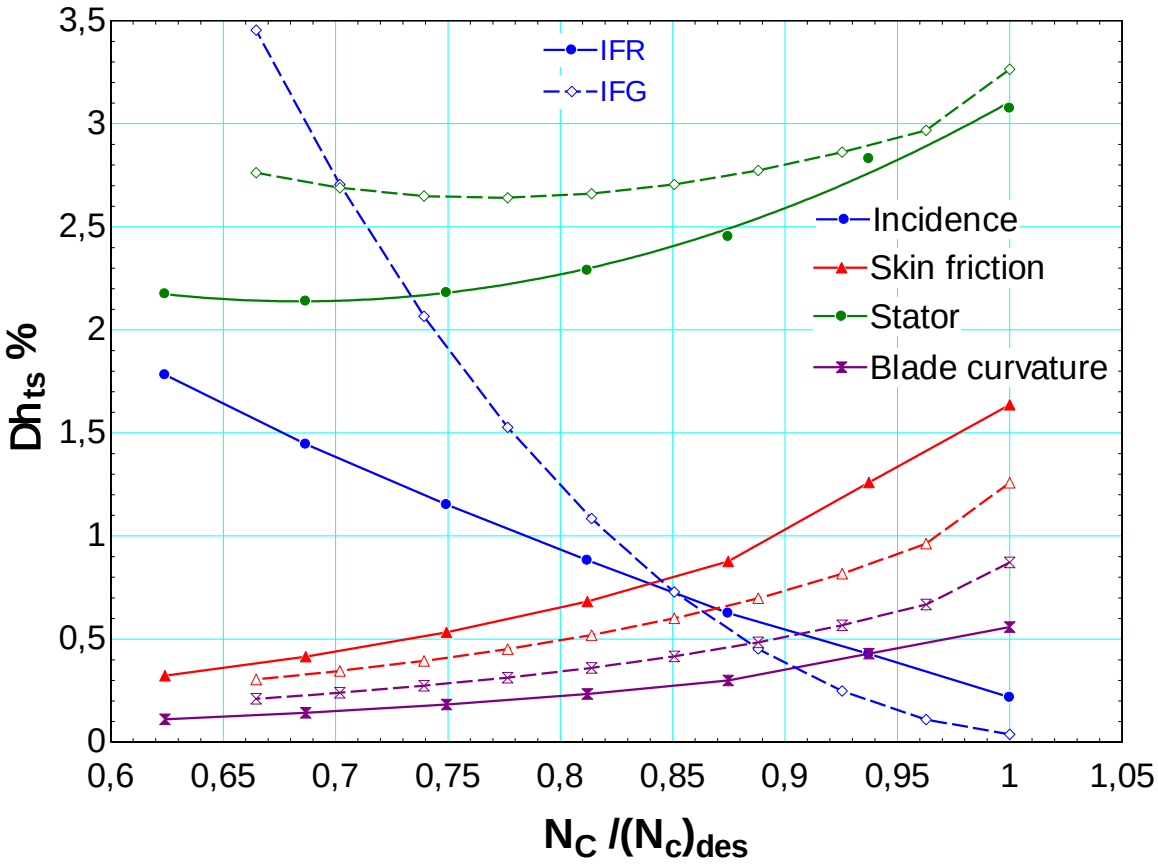

Figure 23 – behavior of total to static efficiency losses ($\Delta\eta_{ts}$) with variable Nc under off design conditions

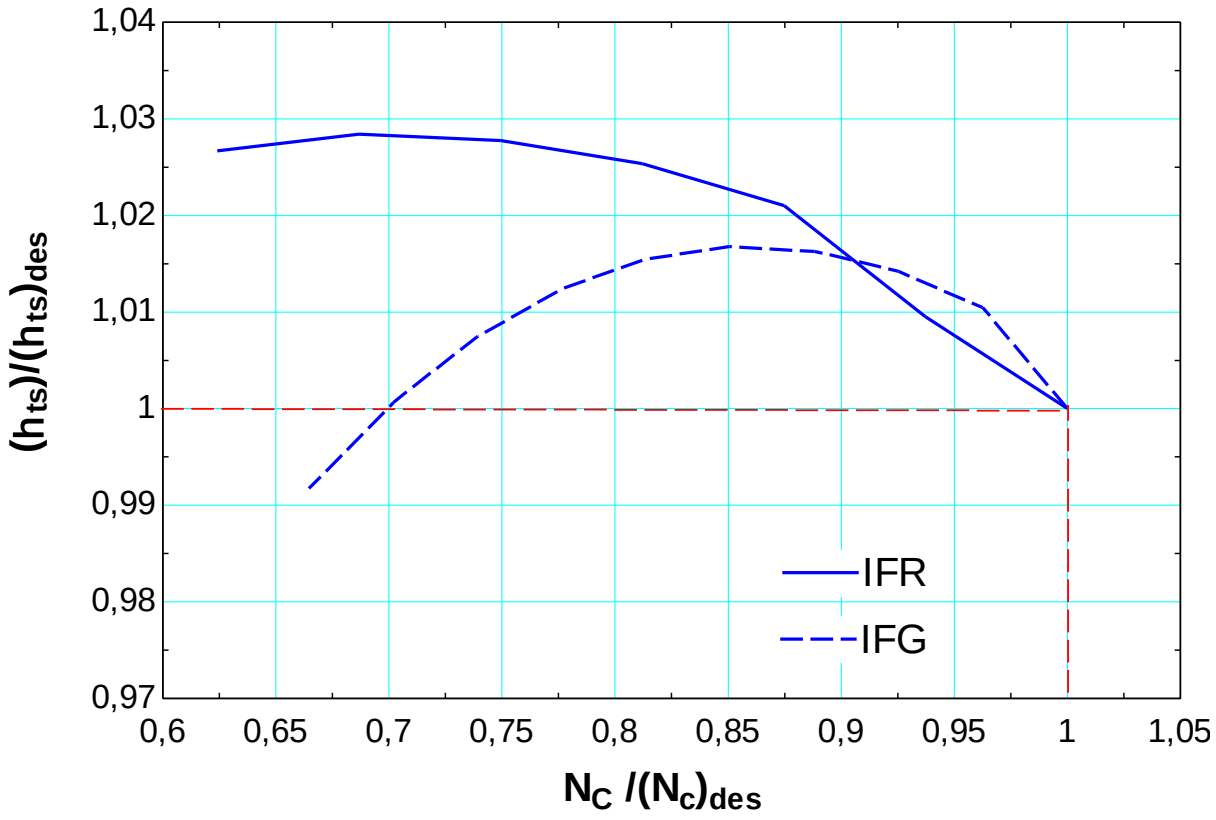

Figure 24 – Total-to-static efficiency vs Nc under off design conditions

854

855 # List of tables

856

857 *Table 1: Input data and typical range of values.*

858

N.	Variable	Typical values
0	Rated Power Output, kW	Variable, typically 5 to 500 kW
1	Fluidname	R134a, R1234yf, R245fa, R236fa, Cyclo-Hexane, N-Pentane
2	Total inlet pressure p_{01} [kPa]	Variable, typically 500 to 4000
3	Total inlet Temperature T_{01} [°C]	Variable, typically 100 - 200
4	Isentropic enthalpy dropΔh_{ss}[kJ/kg]	Variable, typically 28 to 130
5	Work coefficient Ψ	0.90-1.10
6	Flow coefficient Φ	0.13-0.21
7	Isentropic degree of reaction R_s	0.55-0.63
8	Rotor inlet diameter d_2 [m]	0.08-0.195
9	Nozzle geometry ratio d_1/d_2	1.30-1.80
10	Rotor geometry ratio d_3/d_2	0.45 – 0.60
11	Diffuser geometry ratio d_4/d_3	1.4 – 1.6
12	Diffuser length – diameter ratio L_d/d_3	1.5 – 2. 5
13	Rotor aspect ratio b_2/d_2	0.03 – 0.08
14	Nozzle height ratio b_1/b_2	0.8 – 1

859

Fluid Name	**R134a**		**Cyclohexane**		**N-Pentane**		**R245fa**		**R1234yf**		**R236fa**	
Rotor geometry	**IFG**	**IFR**	**IFG**	**IFR**	**IFG**	**IFR**	**IFG**	**IFR**	**IFG**	**IFR**	**IFG**	**IFR**
Rated power output [kW]	50	50	50	50	50	50	50	50	50	50	50	50
Total inlet pressure p_{01} [bar]	38	38	5	5	10	10	31	31	31	31	30	30
Total inlet Temperature T_{01} [°C]	147	147	147	147	147	147	147	147	147	147	147	147
Isentropic enthalpy drop Δh_{ss}[kJ/kg]	38	37	131	132	105	102	54	51	30	28	38	38
Work coefficient Ψ	0.94	1.03	0.93	1.08	0.95	1.05	0.97	1.06	0.91	1.07	0.95	1.04
Flow coefficient Φ	0.21	0.16	0.13	0.16	0.19	0.17	0.16	0.14	0.20	0.14	0.15	0.15
Isentropic degree of reaction R_s	0.61	0.56	0.60	0.57	0.61	0.55	0.61	0.55	0.63	0.55	0.61	0.55
Nozzle geometry ratio d_1/d_2	1.42	1.45	1.73	1.43	1.76	1.74	1.75	1.50	1.42	1.32	1.80	1.72
Rotor geometry ratio d_3/d_2	0.46	0.47	0.55	0.62	0.51	0.54	0.54	0.54	0.56	0.48	0.52	0.55
Diffuser geometry ratio d_4/d_3	1.40	1.40	1.60	1.60	1.40	1.40	1.50	1.50	1.60	1.60	1.50	1.50

Diffuser length – diameter ratio L_d/d_3	2.0	1.5	2.5	2.5	2.0	2.0	2.0	2.0	2.5	2.5	2.0	2.0
Rotor aspect ratio b_2/d_2	0.030	0.045	0.036	0.037	0.042	0.055	0.040	0.046	0.055	0.082	0.049	0.050
Nozzle height ratio b_1/b_2	1.0	1.0	0.8	0.8	1.0	1.0	1.0	1.0	1.0	1.0	1.0	1.0

860

861 *Table 2: Nozzle setting angle as a function of absolute flow angle at nozzle outlet*

862

α_2	α_{b2}
57.5	60
62.1	65
66.5	70
70.9	75
75.2	80

863

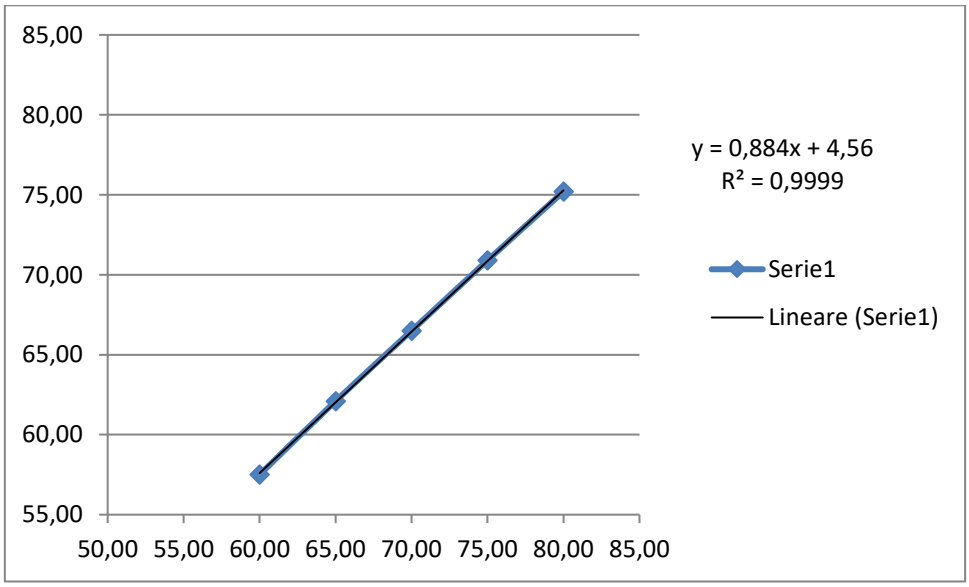

864

865

866

867

868

869

870 *Table 3 – design results of the ORC expander for different working fluids (IFR and IFG)*

Fluid	R134a		Cyclo hexane		N-Pentane		R245fa		R1234yf		R236fa	
	IFR	IFG	IFR	IFG	IFR	IFG	IFR	IFG	IFR	IFG	IFR	IFG
d_1 [m]	0.115	0.115	0.335	0.273	0.188	0.189	0.154	0.138	0.121	0.117	0.157	0.160
d_3 [m]	0.037	0.037	0.106	0.118	0.054	0.059	0.047	0.052	0.047	0.043	0.045	0.050
d_4 [m]	0.052	0.052	0.170	0.189	0.076	0.082	0.071	0.077	0.076	0.068	0.068	0.075
b_1 [m]	0.002	0.004	0.006	0.006	0.005	0.006	0.004	0.004	0.005	0.007	0.004	0.005
b_2 [m]	0.002	0.004	0.007	0.007	0.005	0.006	0.004	0.004	0.005	0.007	0.004	0.005
b_3 [m]	0.013	0.014	0.043	0.050	0.024	0.023	0.021	0.016	0.019	0.016	0.016	0.020
p_{04} [bar]	9.230	9.550	0.149	0.137	0.891	0.930	1.812	2.100	8.109	8.520	3.460	3.450
$\Delta h_{0,stadio}$[kJ/kg]	28.800	28.700	91.700	91.600	74.700	74.700	37.700	37.600	21.700	21.700	27.600	27.900
$\dot{m}$ [kg/s]	1.750	1.749	0.546	0.546	0.672	0.677	1.346	1.349	2.327	2.308	1.815	1.793
u_2 [m/s]	175.1	166.9	313.7	291.2	280.5	266.8	197.4	188.9	154.7	142.6	170.5	164.0
Rpm	41296	40097	30932	29115	50064	46746	42845	39211	34762	30673	37418	33672
α_2 [°]	77.4	81.0	82.1	81.9	78.7	81.1	80.6	82.4	77.6	82.4	81.0	81.8
β_2 [°]	-15.9	10.4	-27.6	27.1	-14.7	16.9	-11.3	21.4	-25.1	26.2	-18.4	14.9
β_3 [°]	-63.9	-65.7	-57.9	-63.3	-56.0	-59.0	-60.8	-60.1	-70.4	-59.5	-59.6	-66.7
$\delta\beta_R$ [°]	48.0	76.1	30.3	90.4	41.3	75.9	49.5	81.5	45.3	85.7	41.2	81.6
M_2	1.047	1.077	1.500	1.626	1.321	1.374	1.441	1.493	0.921	0.982	1.276	1.325
M_3	0.240	0.211	0.563	0.470	0.461	0.412	0.412	0.423	0.190	0.249	0.375	0.277
M_4	0.120	0.106	0.191	0.166	0.216	0.197	0.171	0.174	0.073	0.095	0.157	0.119
M_{r2}	0.237	0.172	0.235	0.261	0.268	0.223	0.240	0.211	0.219	0.144	0.210	0.196
M_{r3}	0.537	0.514	1.059	1.048	0.823	0.802	0.843	0.848	0.566	0.490	0.741	0.696
M_{u2}	1.087	1.032	1.602	1.490	1,363	1,292	1.469	1.403	0.992	0.910	1.327	1.261
M_{u3}	0.480	0.468	0.897	0.936	0.682	0.688	0.736	0.735	0.533	0.422	0.639	0.639
N_s	0.059	0.057	0.095	0.09	0.089	0.080	0.084	0.074	0.073	0.065	0.077	0.067
R	0.52	0.48	0.55	0.47	0.53	0.49	0.52	0.49	0.54	0.47	0.54	0.48
d_{3h}/d_{3s}	0.490	0.443	0.422	0.412	0.393	0.490	0.391	0.520	0.434	0.457	0.479	0.434
Z_B	15	18	21	21	16	18	16	19	15	19	14	18
$\Delta\eta_{ts,N}$ (%)	0.55	0.87	3.75	2.17	1.785	2.37	1.753	1.87	0.692	0.85	1.625	2.02
$\Delta\eta_{ts,i}$(%)	0.22	0.03	0.03	0.19	0.21	0.08	0.27	0.11	0.05	0.20	0.26	0.06
$\Delta\eta_{ts,cl}$(%)	4.59	3.90	5.00	6.48	4.48	2.80	5.00	3.70	3.33	2.22	3.20	4.00
$\Delta\eta_{ts,f}$(%)	1.62	1.25	2.05	1.43	1.80	1.28	2.32	1.30	1.36	0.89	1.32	1.25
$\Delta\eta_{ts,ke}$(%)	1.65	1.33	3.29	2.22	3.31	2.78	2.42	2.78	1.25	2.31	2.68	1.50
$\Delta\eta_{ts,bl}$(%)	11.9	11.27	8.1	9.12	10.8	11.09	11.0	10.63	11.2	11.20	12.77	10.90
$\Delta\eta_{ts,p}$(%)	3.06	3.26	6.49	8.14	5.83	5.80	6.02	5.16	6.79	4.25	4.90	5.03
$\Delta\eta_{ts,df}$(%)	0.72	0.59	1.15	0.81	0.65	0.53	0.67	0.64	0.46	0.39	0.61	0.57
η_{tt}	0.773	0.788	0.733	0.716	0.744	0.760	0.730	0.766	0.761	0.800	0.753	0.76
η_{ts}	0.757	0.775	0.700	0.693	0.711	0.732	0.705	0.738	0.748	0.780	0.726	0.745
$\eta_{ts,eff}$	0.7689	0.784	0.727	0.711	0.736	0.752	0.723	0.760	0.758	0.795	0.747	0.757

871

872

873 **Nomenclature**

874 b blade height [m]

875 BK blockage factor

876 C absolute velocity [m/s]

877 c_s spouting velocity [m/s]

878 d diameter [m]

879 D^* characteristic diameter [m]

880 h enthalpy [J/kg]

881 I rothalpy [J/kg]

882 L^* characteristic length [m]

883 M Mach number

884 $\dot{m}$ mass flow rate [kg/s]

885 N rotational speed [rpm]

886 N_c corrected rotational speed [rpm $K^{1/2}$]

887 $N_s=\frac{N/60\cdot Q_3^{1/2}}{\Delta h_{0s}^{3/4}}$ specific speed

888 p pressure [Pa]

889 q loss coefficient

890 Q volumetric flow rate [m^3/s]

891 r radius [m]

892 Re Reynolds number

893 R Degree of reaction

894 s blade spacing [m]

895 T temperature [K]

896 u peripheral velocity [m/s]

897 w relative velocity [m/s]

898 $\overline{w}$ average relative velocity [m/s]

899 VS sound speed [m/s]

900 V Velocity (general) [m/s]

x	chord [m]
z	axial length of rotor [m]
Z	number of blades

Greeks

α	absolute angle (from radial direction, positive with u) [°]
α_b	actual angle of blades at nozzle outlet
β	relative angle (from radial direction, positive with u) [°]
Δ, δ	variation
ε	clearance[percentage of the blade height]
ε_{ax}	axial disk clearance [m]
ξ	loss coefficient
η	efficiency
λ	frictional factor
μ	dynamic viscosity [Kg/s-m]
ν	kinematic viscosity [m^2/s]
ρ	density [kg/m^3]
$\overline{\rho}$	average density [kg/m^3]
Φ	flow coefficient
Ψ	load coefficient
Ψ_T	Zweifel's coefficient (ratio between the ideal and real tangential load of a blade)
ω	speed of revolution [rad/s]

Subscripts

0	total value (stagnation)
1, 2, 3, 4	referred to sections 1, 2, 3, 4 (figure 4)
act	actual
bl	blade loading
cl	clearance
D	diffuser
df	disk friction
f	friction
h	hub
i	incidence
id	ideal
ke	kinetic energy
le	leading edge
m	meridional (flow rate component)
N	nozzle
opt	optimal
p	profile
R	rotor
r	relative, radial (referring to clearance)
s	isentropic (Nozzle or rotor, h-s diagram)
s	shroud (referred to diameter)
ss	double isentropic (Nozzle + Rotor, h-s diagram)
t	tip

te	trailing edge
u	peripheral

Acronyms

IFR	turbine with Radial blades at rotor inlet (Radial Inlet Flow)
IFG	turbine with General rotor shape at inlet (General Inlet Flow)
ORC	Organic Rankine Cycle

References

[1] Invernizzi, C., Iora, P., Silva, P., 2007, "Bottoming micro-Rankine cycles for micro-gas turbines", *Applied Thermal Engineering,* 27, pp. 100–110

[2] Chacartegui, R., Sánchez, D., Muñoz, J.M., Sánchez, T. , 2009, Alternative ORC bottoming cycles FOR combined cycle power plants, *Applied Energy,* 86 , pp. 2162–2170

[3] Al-Sulaiman,F.A., Dincer, I., Hamdullahpur, F., 2010, "Exergy analysis of an integrated solid oxide fuel cell and organic Rankine cycle for cooling, heating and power production", *Journal of Power Sources,* 195 , pp. 2346–2354

[4] Vaja, I., Gambarotta, A., 2010, "Internal Combustion Engine (ICE) bottoming with Organic Rankine Cycles (ORCs)", *Energy,* 35 , pp. 1084–1093

[5] GE Energy Announces Industrial Waste-Heat Recovery Innovation for Onsite Power Plants, http://www.genewscenter.com/content/detail.aspx?releaseid=7229&newsareaid=2, 6 July, 2009.

[6] "Turboden Combined Heat And Power Orc Units For The Pellet Industries", 2008, http://www.turboden.eu/en/public/press/Turboden_ORC_for_pellets_english.pdf

[7] Schuster, A., Karellas, S., Kakaras, E., Spliethoff, H., 2009, "Energetic and economic investigation of Organic Rankine Cycle applications", *Applied Thermal Engineering,* 29, pp. 1809–1817

[8] Zhai, H., Dai, Y.J., Wu, J.Y., Wang, R.Z. , 2009, "Energy and exergy analyses on a novel hybrid solar heating, cooling and power generation system for remote areas", *Applied Energy,* 86 , pp.1395–1404

[9] Fiaschi, D., Lifshitz, A., Manfrida, G., " Fuel-Assisted Solar Thermal Power Plants with supercritical ORC cycle", Proceedings of ECOS 2010, Lausanne.

[10] Di Pippo, R., 2006, "GeothermalPower Plants: Principles, Applications and Case Studies". Elsevier Advanced Technology, London, UK.

[11] Heberle, F., Brüggemann, D., 2006, "Exergy based fluid selection for a geothermal Organic Rankine Cycle for combined heat and power generation", Applied Thermal Engineering 30, pp. 1326-1332

[12] Lentz, A., Almanza, R., 2006, “Solar–geothermal hybrid system”, *Applied Thermal Engineering* , 26, pp. 1537–1544

[13] Whitfield A., Baines N.C., 1990.”Design of radial turbomachines”, Longman, New York.

[14] Dixon S.L., 1998, ”Fluid Mechanics and Thermodynamics of Turbomachinery”, Butterworth.

[15] Cohen H., Rogers G.F.C., Saravanamuttoo H.I.H.,1996”Gas Turbine Theory”, Longman, New York.

[16] Glassman A.J.,”Turbine Design and Application”, *Scientifical and technical information program-1994,* National Aeronautics and Space Administration (NASA) *Washington, DC.*

[17] Rohlik Harold E., “Analytical Determination of Radial Inflow Turbine Design Geometry for Maximum Efficiency”,National Aeronautics and Space Administration (NASA), Washington, D.C., 1968.

[18] Meitner Peter L., Glassman Arthur J., “ Computer Code for Off-Design Performance Analysis of Radial-Inflow Turbines With Rotor Blade Sweep”, National Aeronautics and Space Administration (NASA), Scientifical and Technical Information Branch, 1983.

[19] Whitfield, A., 1990, “The Preliminary Design of Radial Inflow Turbines”, ASME J. of Turbomachinery, Vol. 112, pp. 51-57.

[20] Rohlik, H. E., 1975, "Radial Inflow Turbines," NASA SP 290, Vol. 3, Ch. 10.

[21] Ainley, D.G. and Mathieson, G.C.R. (1951). “A method of performance estimation for axial flow turbines”, ARC.R. and M.2974.

[22] Wiesner, F.J: "A Review of Slip Factors in Centrifugal Impellers ". J. Eng. Power, vol 89, no. 4, Oct 1967, pp 558-572.

[23] Zweifel, O. (1945). "The spacing of turbomachine blading, especially with large angular deflection. " *Brown Boveri Rev.,* 32,12.

[24] Benson S. Rowland. " A Review of Methods For Assessing Loss Coefficients In Radial Gas Turbines". *Int. J. mech. Sci.* Pergamon Press. 1970. Vol 12, pp 905-932.

[25] Hiett G.F. and Johnston I.H., Proc. Inst. Mech. Engrs 178, part 31 (1963-64).

[26] Balje O.E. " A Contribution to the Problem of Designing Radial Turbomachines ", *Trans. A.S.M.E.* 741, 451 (1952).

[27] Bridle E.A., Boulter R.A., " A Simple Theory for the Prediction of Losses in the Rotors of Inward Radial Flow Turbines ", Procediings of the institution of mechanical engineers, conference procediings 1964-1970 (vols 178-184), 1967.

[28] Futral Samuel M., Jr., Wasserbauer Charles A., " Off Design Performance Prediction with Experimental Verification for a Radial-Inflow Turbine ", *Lewis Research Center Cleveland, Ohio,* National Aeronautics and Space Administration, Washington, D.C. February 1965.

[29] Hiett, G. F. and Johnston, I. H. " Experiments Concerning the Aerodynamic Performance of Inward Flow Radial Turbines ", Paper 7, *Thermodynamics and Fluid Mechanics Conv., Proc. Instn mech. Engrs 1963-64 178 (Pt 3 I (ii), 28.*

[30] Futral Samuel M., Jr., and Holeski Donald E., " Experimental Results of Varying the Blade-Shroud Clearance in a 6.02-Inch Radial-Inflow Turbine ", *Lewis Research Center Cleveland, Ohio,* National Aeronautics and Space Administration, Washington, D.C. January 1970.

[31] Atlas Copco Gas and Process Division, "Driving Expander Technology", http://www.atlascopco-gap.com/download_file.php?id=457

[32] GE Energy Oil & Gas, TurboExpanders/Generators for NaturalGas Applications, http://www.geoilandgas.com/businesses/ge_oilandgas/en/prod_serv/prod/turboexpanders/en/downloads/turboexpanders.pdf

[33] Pratt&Whitney Power Systems, "Organic Rankine Cycle Technology", http://www.pw.utc.com/StaticFiles/Pratt%20&%20Whitney%20New/Media%20Center/Assets/1%20Static%20Files/Docs/pwps_orc_brochure_2010.pdf

[34]http://www.fchart.com/ees/

[35]http://www.fchart.com/ees/ees-refprop.php, http://www.nist.gov/srd/nist23.cfm

[36] Manfrida, G., Tempesti, D., 2011, "Maximum exergy control of micro-CHP systems operating with geothermal and solar energy", ICAE 2011 Conference, Perugia.

[37] Daniele Fiaschi, Giampaolo Manfrida and Francesco Maraschiello, "Thermo-fluid dynamics preliminary design of turbo-expanders for ORC cycles",Applied Energy, Volume 97, September 2012, Pages 601-608.

[38] Balje O. E.:"Turbomachines. A Guide to Design, Selection and Theory", 1981, Wiley.

[39] Deng QingHua, Niu JiuFang & Feng ZhenPing, " Study on Leakage Flow Characteristics of Radial Inflow Turbines at Rotor Tip Clearance ", 2008, *Science in China Series E: Technological Sciences*, Springer.

[40] Rodgers, C., Geiser, T., 1987, Performance of a High-Efficiency Radial/Axial Turbine, ASME J. of Turbomachinery, 109, pp. 151-154.

[41] Idelc'ijk, 1978, " Memento des pertes de charge ", Eyrolles

[42] Runstadler, P.W., Dolan, F.X., Dean, R.C., 1974, " Diffuser Data Book ", CREARE Inc.